

# Rethinking Spectral Graph Neural Networks with Spatially Adaptive Filtering

**Jingwei Guo\***

University of Liverpool  
Liverpool, UK

jingwei.guo@liverpool.ac.uk

**Kaizhu Huang<sup>†</sup>**

Duke Kunshan University  
Suzhou, China

kaizhu.huang@dukekunshan.edu.cn

**Xinping Yi**

Southeast University  
Nanjing, China

xyi@seu.edu.cn

**Zixian Su\***

University of Liverpool  
Liverpool, UK

zixian.su@liverpool.ac.uk

**Rui Zhang**

Xi'an Jiaotong-Liverpool University  
Suzhou, China

rui.zhang02@xjtlu.edu.cn

## Abstract

Whilst spectral Graph Neural Networks (GNNs) are theoretically well-founded in the spectral domain, their practical reliance on polynomial approximation implies a profound linkage to the spatial domain. As previous studies rarely examine spectral GNNs from the spatial perspective, their spatial-domain interpretability remains elusive, *e.g.*, what information is essentially encoded by spectral GNNs in the spatial domain? In this paper, to answer this question, we investigate the theoretical connection between spectral filtering and spatial aggregation, unveiling an intrinsic interaction that spectral filtering implicitly leads the original graph to an adapted new graph, explicitly computed for spatial aggregation. Both theoretical and empirical investigations reveal that the adapted new graph not only exhibits non-locality but also accommodates signed edge weights to reflect label consistency among nodes. These findings thus highlight the interpretable role of spectral GNNs in the spatial domain and inspire us to rethink graph spectral filters beyond the fixed-order polynomials, which neglect global information. Built upon the theoretical findings, we revisit the state-of-the-art spectral GNNs and propose a novel Spatially Adaptive Filtering (SAF) framework, which leverages the adapted new graph by spectral filtering for an auxiliary non-local aggregation. Notably, our SAF comprehensively models both node similarity and dissimilarity from a global perspective, therefore alleviating persistent deficiencies of GNNs related to long-range dependencies and graph heterophily. Extensive experiments over 13 node classification benchmarks demonstrate the superiority of our proposed framework to the state-of-the-art methods.

## 1 Introduction

Graph Neural Networks (GNNs) have shown remarkable abilities to uncover the intricate dependencies within graph-structured data, and achieved tremendous success in graph machine learning [1, 2, 3]. Spectral GNNs are a class of GNNs rooted in spectral graph theory [4, 5], implementing graph convolutions via spectral filters [6, 7]. Whilst various spectral filtering strategies [8, 9, 10, 11, 12, 13, 14, 15, 16] have been proposed for spectral GNNs, their practical implementations invariably resort to approximating graph filters with fixed-order polynomials for computational

\*Also with Xi'an Jiaotong-Liverpool University.

<sup>†</sup>Corresponding Author

efficiency [13, 12]. This truncated approach essentially relies on the direct extraction of spatial features from the local regions of nodes. As such, the spatial domain of a graph, albeit loosely connected to spectral GNNs in theory, still plays a crucial role in effectively learning node representations.

However, there is a notable lack of research examining spectral GNNs from the spatial perspective. Though recent studies analyze both spectral and spatial GNNs to elucidate their similarities in model formulations [17, 18, 19], outcomes [20, 21], and expressiveness [22, 23, 13, 24], they neglect the interpretability that could arise mutually from the other domain. Specifically, while most spectral GNNs have well explained their learned filters in the spectral domain [10, 13, 12, 14], understandings from the spatial viewpoint are merely limited to fusing multi-scale graph information [25]; this unfortunately lacks a deeper level of interpretability in the vertex domain. Therefore, a natural question arises: *what information is essentially encoded by spectral GNNs in the spatial domain?*

In this work, we attempt to answer this question by exploring the connection between spectral filtering and spatial aggregation. The former is the key component in spectral GNNs, while the latter is closely associated with spatial GNNs utilizing recursive neighborhood aggregation. In existing GNN frameworks, these two approaches rarely interact each other at the risk of domain information trade-offs due to uncertainty principles [26, 27, 28]. Recognizing the spatial significance in spectral filtering, He et al. [10] have recently considered non-negative constraints as part of a generalized graph optimization problem. Notably, however, spatial aggregation meanwhile resembles the optimizing trajectory of the same optimization problem through iterative steps, which may be easily overlooked. Inspired by such observation, we examine, for the first time, the theoretical interaction between spectral filtering and spatial aggregation. This exploration has led us to uncover an intriguing theoretical interplay, *i.e.*, spectral filtering implicitly modifies the original graph, transforming it into a new one that explicitly functions as a computation graph for spatial aggregation. Delving deeper, we discover that the adapted new graph enjoys some desirable properties, enabling a direct link among nodes that originally require multiple hops to do so, thereby exhibiting nice non-locality. Moreover, we find that the new graph edges allow signed weights, which turns out capable of distinguishing between label agreement and disagreement of the connected nodes.

Overall, these findings underscore the interpretable role and significance of spectral GNNs in the spatial domain, inspiring us to rethink graph spectral filters beyond the fixed-order polynomials, which limit models’ effective propagation range and hinder their ability to capture long-range dependencies. Concretely, we propose a novel Spatially Adaptive Filtering (SAF) framework to fully explore spectral GNNs in the spatial domain. SAF leverages the adapted new graph by spectral filtering for auxiliary spatial aggregation and allows individual nodes to flexibly balance between spectral and spatial features. By performing non-local aggregation with signed edge weights, SAF adeptly overcomes the limitations of truncated polynomials, enabling the model to capture both node similarity and dissimilarity at a global scale. As a benefit, it can mitigate persistent deficiencies of GNNs regarding long-range dependencies and graph heterophily. The contributions are summarized as follows:

- Our investigation into spectral GNNs in the spatial domain reveals that they fundamentally alters the original graph, introducing non-locality and signed edge weights to discern node label consistency.
- We propose Spatially Adaptive Filtering (SAF) framework, a paradigm-shifting approach to spectral GNNs that jointly leverages graph learning in both spatial and spectral domains, making it a powerful tool for capturing long-range dependencies and handling graph heterophily.
- Extensive experiments over 13 node classification benchmarks exhibit notable improvements of up to 15.37%, and show that SAF beats the best-performing spectral GNNs on average.

## 2 Related Works

**Graph Neural Networks.** GNNs can be broadly divided into spatial-based and spectral-based methods. Spatial GNNs leverage the spatial connections among nodes to perform message passing, also known as spatial aggregation [29, 30] (see works [31, 1] for a thorough review). Spectral GNNs leverage the graph’s spectral domain for convolution or, alternatively, spectral filtering [7, 32]. Prevailing approaches focus on developing polynomial graph filters, by either learning polynomial coefficients, such as GPR-GNN [9], BernNet [10], ChebNetII [12], and JacobiConv [13], or optimizing the polynomial basis for better adaption, as seen in models like LON-GNN [15] and OptBasisGNN [16]. Diverging from this trend, ARMA [33] employs rational filter functions while still approximating

them with polynomials. Although these methods are theoretically grounded in the spectral domain, their practical reliance on polynomial approximation hints at a profound linkage to the spatial domain. However, the spatial-domain interpretation of spectral GNNs is rarely examined. To this end, we delve into in this paper the intrinsic information spectral GNNs convey within the spatial context.

**Unified Viewpoints for GNNs.** Several works have explored the nuances between spatial and spectral GNNs. Early studies by Balcilar et al. [17] and Chen et al. [18] examined their similarities in model formulations. Chen et al. [22] proved their spatial GNN’s anti-oversmoothing ability via spectral analysis. Ma et al. [20] and Zhu et al. [21] utilized the graph signal denoising problem to integrate both GNN types, and their expressiveness equivalence is further explored in works [23, 13]. Recently, Sun et al. [24] have highlighted the feature space constraints of both spatial and spectral GNNs, while Guo and Wei [19] tend to emphasize their relationship via residual connection. Though these studies effectively bridge spectral and spatial GNNs, they remain focused on congruencies. Unlike them, our work represents the first endeavor to delve into the interpretability of spectral GNNs in the spatial domain, emphasizing the theoretical synergy between spectral filtering and spatial aggregation. The empirical success of our method (as compared to unified GNNs in Tables 1 and 2), stem from this in-depth analysis, further underscoring our practical contributions to the literature.

**Long-range Dependencies.** While substantial efforts have been directed towards capturing long-range dependencies in spatial GNNs [34, 22, 35, 36, 37, 38], the exploration of the same challenge in spectral GNNs remains under-studied. To fill this gap, we propose SAF framework, which emerges as a valuable consequence of analyzing spectral GNNs in the spatial domain, enhancing their long-range dependency capture. Aligned with our objective, Bo et al. [39] introduced Specformer to addresses long-range dependencies for spectral GNNs, using a Transformer based set-to-set spectral filter. However, it lacks spatial-domain interpretability and introduce more trainable parameters. In contrast, our approach creates a non-local new graph without learning additional parameters, meanwhile elucidating the spatial implications of spectral GNNs. Similarly, a recent approach, FLODE [40], also produces matrices capable of capturing long-range dependencies by utilizing the fractional graph Laplacian [41]. However, this work mainly generalizes existing concepts from undirected to directed graphs to mitigate graph oversmoothing. Our study, conversely, focuses on exploring the fundamental issues surrounding undirected graphs to delve deeper into the intrinsic significance of spectral GNNs.

**Graph Heterophily.** Graph heterophily [36, 42], where different labeled nodes connect, challenges GNNs operating under the homophily assumption [43]. Although many GNNs have been crafted to manage heterophilic connections [44, 45, 9, 46, 47, 48], our method offers a distinct solution. Specifically, SAF innovatively conducts an auxiliary non-local aggregation using signed edge weights, emphasizing both intra-class similarity and inter-class difference on a global scale. One should note that there are two recent works [49, 50] also employ signed edge weights, introducing GloGNN and LRGNN, respectively. GloGNN aims to capture global homophily but is limited to K-hop neighborhood information, while LRGNN extends this by using low-rank properties to approximate the true global relationships between node labels. Despite their success, both methods focus primarily on fitting node label relationships without fully exploring the fundamental GNN mechanisms, leading to a heavy reliance on label supervision (see Appendix F.2). Differently, our SAF leverages cross-domain insights into GNNs, ensuring the theoretical soundness of non-local learning, as proven in Section 4.2. This allows SAF to consistently perform well under both sparse and dense supervision.

### 3 Preliminaries

**Notations.** Let  $\mathcal{G} = (\mathcal{V}, \mathcal{E})$  be a graph with node set  $\mathcal{V}$  and edge set  $\mathcal{E}$ , where the number of nodes is denoted by  $N$ . The adjacency matrix  $\mathbf{A} \in \mathbb{R}^{N \times N}$  defines the edge weights  $A_{i,j}$  between nodes  $v_i$  and  $v_j$ , and the degree matrix  $\mathbf{D}$  can be obtained by summing the rows of  $\mathbf{A}$  into a diagonal matrix. We denote the graph Laplacian matrix as  $\mathbf{L}$ , which is often normalized into  $\hat{\mathbf{L}} = \mathbf{I} - \hat{\mathbf{A}}$  with  $\hat{\mathbf{A}} = \mathbf{D}^{-\frac{1}{2}} \mathbf{A} \mathbf{D}^{-\frac{1}{2}}$  and an identity matrix  $\mathbf{I}$ . Let  $\hat{\mathbf{L}} = \mathbf{U} \mathbf{\Lambda} \mathbf{U}^T$  be the Laplacian eigendecomposition, where  $\mathbf{U}$  is eigenvector matrix and  $\mathbf{\Lambda} = \text{diag}(\lambda_1, \lambda_2, \dots, \lambda_N)$  consists of eigenvalues within  $[0, 2]$ . For node classification, we usually have a feature matrix  $\mathbf{X} \in \mathbb{R}^{N \times F}$  with  $F$  being raw feature dimensions, and each node is assigned a one-hot label vector  $\mathbf{y}_i \in \mathbb{R}^C$  where  $C \leq N$  is class number.

**Spectral Filtering.** Spectral filtering is essential in spectral GNNs. It selectively shrinks or amplifies the Fourier coefficients of node features [6] for learning tasks and usually take the form as

$$\mathbf{Z} = g_\psi(\hat{\mathbf{L}}) \mathbf{X} = \mathbf{U} g_\psi(\mathbf{\Lambda}) \mathbf{U}^T \mathbf{X}. \quad (1)$$

Here,  $g_\psi : [0, 2] \rightarrow \mathbb{R}$  defines a graph filter function, which are often approximated by a  $K$ -order polynomial in practice. Specifically, we have  $g_\psi(\lambda) = \sum_{k=0}^K \psi_k P_k(\lambda) = \sum_{k=0}^K \omega_k \lambda^k$  where  $P_k : [0, 2] \rightarrow \mathbb{R}$  refers to a polynomial basis and both  $\psi_k$  and  $\omega_k$  denote the polynomial coefficient.

**Spatial Aggregation.** Spatial aggregation is a central component of spatial GNNs, facilitating the propagation of node information along edges and its subsequent aggregation within node neighborhood. To provide a better illustration, let's consider a popular spatial GNN, APPNP [34]. This model begins with a feature transformation  $\mathbf{Z}^{(0)} = f(\mathbf{X})$ , and then perform the spatial aggregation as:

$$\mathbf{Z}^{(k)} = (1 - \eta)\mathbf{Z}^{(0)} + \eta \hat{\mathbf{A}} \mathbf{Z}^{(k-1)}, \quad k = 1, 2, \dots, K, \quad (2)$$

where  $\hat{\mathbf{A}} = \tilde{\mathbf{D}}^{-\frac{1}{2}} \tilde{\mathbf{A}} \tilde{\mathbf{D}}^{-\frac{1}{2}}$ ,  $\tilde{\mathbf{A}} = \mathbf{A} + \mathbf{I}$ , and  $\eta$  refers to the update rate.

## 4 Rethinking Spectral GNNs from the Spatial Perspective

In this section, we provide both theoretical and empirical analyses to examine spectral GNNs from the spatial perspective and answer the question, *i.e.*, what information is essentially encoded by spectral GNNs in the spatial domain?

### 4.1 Interplay of Spectral and Spatial Domains through the Lens of Graph Optimization

The graph signal denoising problem [5] was initially leveraged in [20, 21] as a means to interpret GNNs with smoothness assumption, which yet does not always hold in certain real-world graph scenarios such as heterophily [42]. Without loss of generality, in this work, we consider a more generalized graph optimization problem<sup>3</sup>

$$\arg \min_{\mathbf{Z}} \mathcal{L} = \alpha \|\mathbf{X} - \mathbf{Z}\|_F^2 + (1 - \alpha) \cdot \text{tr}(\mathbf{Z}^T \gamma_\theta(\hat{\mathbf{L}}) \mathbf{Z}) \quad (3)$$

where  $\mathbf{Z} \in \mathbb{R}^{N \times d}$  refers to node representations,  $\gamma_\theta(\hat{\mathbf{L}})$  determines the rate of propagation [51] by operating on the graph spectrum, *i.e.*,  $\gamma_\theta(\hat{\mathbf{L}}) = \mathbf{U} \gamma_\theta(\mathbf{\Lambda}) \mathbf{U}^T$ , and  $\alpha \in (0, 1)$  is a trade-off coefficient. In case of setting  $\gamma_\theta(\hat{\mathbf{L}}) = \hat{\mathbf{L}}$ , Eq. (3) turns into the well-known graph signal denoising problem. To ensure the convexity of the objective in Eq. (3), a positive semi-definite constraint is imposed on  $\gamma_\theta(\hat{\mathbf{L}})$ , *i.e.*,  $\gamma_\theta(\lambda) \geq 0$  for  $\lambda \in [0, 2]$ . Then, one can address this minimization problem through either closed-form or iterative solutions.

**Closed-form Solution.** The closed-form solution can be obtained by setting the derivative of the objective function  $\mathcal{L}$  to 0, *i.e.*,  $\frac{\partial \mathcal{L}}{\partial \mathbf{Z}} = 2\alpha(\mathbf{Z} - \mathbf{X}) + 2(1 - \alpha)\gamma_\theta(\hat{\mathbf{L}})\mathbf{Z} = 0$ . Let  $g_\psi(\lambda) = (1 + \frac{1-\alpha}{\alpha}\gamma_\theta(\lambda))^{-1}$ , we can observe that the closed-form solution in Eq. (4) is equivalent to the spectral filtering in Eq. (1).

$$\mathbf{Z}^* = (\mathbf{I} + \frac{1-\alpha}{\alpha}\gamma_\theta(\hat{\mathbf{L}}))^{-1} \mathbf{X} = g_\psi(\hat{\mathbf{L}}) \mathbf{X} = \mathbf{U} g_\psi(\mathbf{\Lambda}) \mathbf{U}^T \mathbf{X}. \quad (4)$$

As  $\gamma_\theta(\lambda) \geq 0$ , this establishes a more stringent constraint for the graph filter in spectral GNNs, *i.e.*,  $0 < g_\psi(\lambda) \leq \frac{\alpha}{\alpha + (1-\alpha) \cdot 0} = 1$ , which is termed as a non-negative constraint in this paper.

**Iterative Solution.** Alternatively, we can take an iterative gradient descent method such that  $\mathbf{Z}^{(k)} = \mathbf{Z}^{(k-1)} - b \frac{\partial \mathcal{L}}{\partial \mathbf{Z}}|_{\mathbf{Z}=\mathbf{Z}^{(k-1)}}$  with a step size  $b = \frac{1}{2}$ , which yields a concise iterative solution in Eq. (5) with  $\hat{\mathbf{A}}^{\text{new}} = \mathbf{I} - \gamma_\theta(\hat{\mathbf{L}})$ . Notably, by taking  $\hat{\mathbf{A}}^{\text{new}}$  as a new computation graph, this solution closely mirrors the spatial aggregation in Eq. (2).

$$\mathbf{Z}^{(k)} = \alpha \mathbf{X} + (1 - \alpha) \hat{\mathbf{A}}^{\text{new}} \mathbf{Z}^{(k-1)}, \quad k = 1, 2, \dots, K \quad (5)$$

**Theoretical Interaction — the Adapted New Graph.** With the non-negative constraint, it is evident that both spectral filtering and spatial aggregation effectively address the generalized graph optimization problem in Eq. (3), despite their distinctive forms and operation domains. Upon closer

<sup>3</sup>This problem was first introduced in [10] for theoretically grounded graph filters. However, in this study, we repurpose it as a bridge between spectral filtering and spatial aggregation.

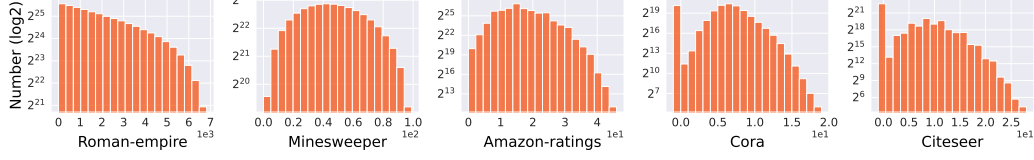


Figure 1: Distributions of connected nodes in the new graph based on their geodesic/shortest-path distance (as  $\Delta_{i,j}$ ) in the original graph. Nodes, distant in the original graph ( $\Delta_{i,j} > 1$  in x-axis), can be linked in the new graph (Number  $> 0$  in y-axis).

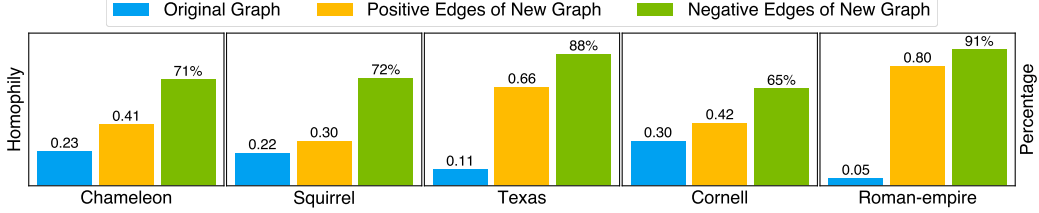


Figure 2: Left y-axis: Homophily comparison between original and new graphs, considering only positive edges (blue and yellow bars). Right y-axis: Percentage of negative edges in the new graph that connect nodes from different classes (green bar).

examination, we discover a compelling relationship between the graph filter  $g_\psi(\lambda)$  in Eq. (4) and the new graph  $\hat{\mathbf{A}}^{\text{new}}$  in Eq. (5), given  $g_\psi(\lambda) = (1 + \frac{1-\alpha}{\alpha}\gamma_\theta(\lambda))^{-1}$ ,

$$\hat{\mathbf{A}}^{\text{new}} = \mathbf{I} - \gamma_\theta(\hat{\mathbf{L}}) = \mathbf{I} - \frac{\alpha}{1-\alpha}(g_\psi(\hat{\mathbf{L}})^{-1} - \mathbf{I}) \quad (6)$$

which unveils an intrinsic inter-play, *i.e.*, spectral filtering implicitly leads the original graph to an adapted new graph, explicitly computed for spatial aggregation.

**What are the differences between  $\hat{\mathbf{A}}^{\text{new}}$  and  $g_\psi(\hat{\mathbf{L}})$ ?** Whereas the former as the uncovered new graph elucidates the inherent spatial node relationships, the latter is a operation in spectral GNNs that processes graph features within spectral domain. It is crucial to understand that  $g_\psi(\hat{\mathbf{L}})$  may not result in a dense matrix, especially with fixed-order polynomial approximation. This is because it captures up to only a  $K$ -hop neighborhood, *i.e.*,  $g_\psi(\hat{\mathbf{L}}) = \sum_{k=0}^K \psi_k P_k(\hat{\mathbf{L}}) = \sum_{k=0}^K \omega_k \hat{\mathbf{A}}^k$ , practically limiting spectral GNNs' effective propagation range. In contrast, our newfound graph  $\hat{\mathbf{A}}^{\text{new}}$  intrinsically enjoys a non-local property, as confirmed in the following section. Building upon this discovery, we further devise a framework to transcend domain barriers, overcoming the limitations of current spectral GNNs due to truncated polynomials (see details in Section 5).

## 4.2 In-depth Analysis of the Adapted New Graph

To deepen our understanding of the interpretability produced by spectral GNNs in the spatial domain, we embark upon a blend of theoretical and empirical inquiries into the adapted new graph.

**Non-locality.** Our examination of the adapted new graph illuminates its non-local nature, particularly evident in the infinite series expansion of the original graph's adjacency matrix. To elucidate, we first introduce a pivotal mathematical construct, the Neumann series, in the following lemma.

**Lemma 1.** *Let  $\mathbf{M} \in \mathbb{R}^{N \times N}$  be a matrix with eigenvalues  $\lambda_n$ , if  $|\lambda_n| < 1$  for all  $n = 1, 2, \dots, N$ , then  $(\mathbf{I} - \mathbf{M})^{-1}$  exists and can be expanded as an infinite series, *i.e.*,  $(\mathbf{I} - \mathbf{M})^{-1} = \sum_{t=0}^{\infty} \mathbf{M}^t$ , which is known as Neumann series.*

With the established non-negative constraint on graph filters, specifically  $0 < g_\psi(\lambda) \leq 1$ , it becomes evident that the eigenvalues of  $\mathbf{I} - g_\psi(\hat{\mathbf{L}})$  falls into the interval permitting Neumann series expansion, as shown in lemma 1 [52]. Building on this observation, we present a non-trivial property of the new graph in the following proposition (see proof in Appendix B.1).

**Proposition 1.** *Given adjacency matrix  $\hat{\mathbf{A}}^{\text{new}}$  formulated in Eq. (6), the adapted new graph exhibits non-locality. Specifically,  $\hat{\mathbf{A}}^{\text{new}}$  is expressible as an infinite series expansion of the original graph's*

adjacency matrix  $\hat{\mathbf{A}}$ . Formally, we have  $\hat{\mathbf{A}}^{new} = \mathbf{I} - \frac{\alpha}{1-\alpha} \sum_{t=1}^{\infty} (\mathbf{I} - \sum_{k=0}^K \pi_k \hat{\mathbf{A}}^k)^t = \sum_{t=0}^{\infty} \phi_t \hat{\mathbf{A}}^t$  where  $\pi_k$  and  $\phi_t$  refer to the constant coefficients computed from  $\{\psi_0, \psi_1, \dots, \psi_K\}$  in distinct ways.

This proposition implies that the new graph engenders immediate links between nodes that originally necessitate multiple hops for connection. To further underpin this theoretical claim, we analyze the general connection status on the new graph by BernNet [10], a spectral GNN adhering to the non-negative constraint. From Figure 1, it is apparent that nodes originally separated by multiple hops achieve direct connections in the new graph.

**Signed Edge Weights — Discerning Label Consistency.** Upon further scrutinizing the adapted new graph, we make a notable discovery that it readily accommodates both positive and negative edge weights. A more granular analysis in Figure 2 reveals that a considerable portion of positive edge weights are assigned to the same-class node pairs, enhancing graph homophily (exemplified by edge homophily ratio [42]). Conversely, edges parameterized with negative weights tend to bridge nodes with different labels. These findings demonstrate the newfound graph’s adeptness in discerning label consistency among nodes. To theoretically explain this phenomenon, we further present the proposition below (see proof in Appendix B.2):

**Proposition 2.** *Let  $\mathbf{Z}^*$  be the node representations optimized by Eq. (3). For  $\mathbf{Z}^*$  to be effective in label prediction, it is a necessary condition that  $\hat{\mathbf{A}}^{new}$  accommodates both positive and negative edge weights s.t. for any node pairs  $v_i, v_j \in \mathcal{V}$ ,  $\hat{A}_{i,j}^{new} > 0$  if  $\mathbf{y}_i = \mathbf{y}_j$  and  $\hat{A}_{i,j}^{new} < 0$  if  $\mathbf{y}_i \neq \mathbf{y}_j$ .*

Proposition 2 provides a theoretical foundation of our empirical findings on the new graph. The essence lies in the objective in Eq. (3), particularly the trace term  $\text{tr}(\mathbf{Z}^T \gamma_{\theta}(\hat{\mathbf{L}}) \mathbf{Z})$ . For clarity, let us reinterpret this trace term as  $\text{tr}(\bar{\mathbf{Z}}^T (\mathbf{D}^{new} - \mathbf{A}^{new}) \bar{\mathbf{Z}})$ , where  $\mathbf{D}^{new}$  denotes the related degree matrix and  $\bar{\mathbf{Z}}$  is derived from rescaling  $\mathbf{Z}$ . Clearly, this term evaluates label smoothness among adjacent nodes in the new graph, which, given its non-local nature, includes both intra-class ( $=$ ) and inter-class ( $\neq$ ) node connections such that  $\mathbf{A}^{new} = \mathbf{A}_{=}^{new} + \mathbf{A}_{\neq}^{new}$ . Drawing from proposition 2, we can further dissect the original trace term, splitting it into  $\text{tr}(\bar{\mathbf{Z}}^T (\mathbf{D}_{=}^{new} - \mathbf{A}_{=}^{new}) \bar{\mathbf{Z}}) - \text{tr}(\bar{\mathbf{Z}}^T |(\mathbf{D}_{\neq}^{new} - \mathbf{A}_{\neq}^{new})| \bar{\mathbf{Z}})$  where the  $|\cdot|$  operation denotes absolute values. As such, it becomes evident that minimizing this trace term not only enhances the representational proximity for same-class node pairs but also strengthens the distinctiveness for different-class nodes pairs. Such nuanced behaviors, inherent to the optimization in Eq. (3), are necessary for GNN models to achieve accurate label predictions.

To summarize, our investigation into spectral GNNs in the spatial domain reveals that they fundamentally alters the original graph, imbuing it with non-locality and signed edge weights that capture label relationships among nodes. These findings highlight the interpretable role of spectral GNNs in the spatial domain and prompt us to rethink current models beyond the truncated polynomial filters.

## 5 Spatially Adaptive Filtering Framework

Building on our discoveries, we re-evaluate the state-of-the-art spectral GNNs and put forth a paradigm-shifting framework, Spatially Adaptive Filtering (SAF), for joint exploitation of graph-structured data across both spectral and spatial domains. SAF leverages the adapted new graph by spectral filtering for an auxiliary non-local aggregation, addressing enduring challenges in GNNs related to long-range dependencies and graph heterophily. See the overall pipeline in Appendix A.

**Non-negative Spectral Filtering.** The proposed SAF requires explicit computation of the newfound graph, as outlined in Eq. (6). This further necessitates the graph filter  $g_{\psi} : [0, 2] \rightarrow \mathbb{R}$  to satisfy the non-negative constraint from Eq. (3):  $0 \leq g_{\psi}(\lambda) \leq 1$ . However, not all extant graph filters fulfill this prerequisite. For instance, the filter use by GCN [7],  $g_{\psi}(\lambda) = 1 - \lambda$ , takes negative values when  $\lambda > 1$ . In this research, we approximate the graph filter using Bernstein polynomials [53], which are known for their non-negative traits [54] and are essential in a preeminent spectral GNN, BernNet [10]. For  $g_{\psi}(\lambda) \leq 1$  part, we rescale Bernstein polynomials with the following proposition.

**Proposition 3.** *Let  $B_{k,K}(x)$  denote the Bernstein polynomial basis of index  $k$  and order  $K$ , which is defined as  $B_{k,K}(x) = \binom{K}{k} (1-x)^{K-k} x^k$  for  $x \in [0, 1]$ . Let  $\psi_k$  denote the  $k$ -th coefficient of a polynomial  $p(x)$  of order  $K$ , where  $p(x) = \sum_{k=0}^K \psi_k B_{k,K}(x)$  with  $\psi_k \geq 0$  for all  $k$ . Then for all  $x \in [0, 1]$ , we have  $g_{\psi}(x) \leq \max\{\psi_k\}_{k=0}^K$ .*

Proposition 3 suggests that the Bernstein polynomial function attains its maximum value in  $\psi_{\max} = \max\{\psi_k\}_{k=0}^K$ . Therefore,  $g_\psi(\lambda)$  can be rescaled within  $[0, 1]$  by  $\hat{g}_\psi(\lambda) = \frac{1}{\psi_{\max}} \sum_{k=0}^K \psi_k B_{k,K}(\frac{\lambda}{2})$ , which enables us to formulate the spectral filtering in SAF as  $\mathbf{Z}_f = \hat{g}_\psi(\hat{\mathbf{L}})f_\varphi(\mathbf{X}) = \frac{1}{\psi_{\max}} \sum_{k=0}^K \psi_k \frac{1}{2^K} \binom{K}{k} (2\mathbf{I} - \hat{\mathbf{L}})^{K-k} \hat{\mathbf{L}}^k f_\varphi(\mathbf{X})$  where  $f_\varphi(\cdot)$ , a two-layer MLP, maps  $\mathbf{X}$  from  $F$  to  $C'$  dimensions using 64 hidden units, and  $\{\psi_k\}_{k=1}^K$  are non-negative learnable parameters. Note that SAF also permits alternative implementations such as using Chebyshev polynomials [55, 6] for graph filter learning, enhancing models like ChebNetII [12] (see details in Appendix F.6).

**Non-local Spatial Aggregation.** Once acquiring a suitable spectral filter  $\hat{g}_\psi(\lambda)$ , we compute the adapted new graph as  $\hat{\mathbf{A}}^{\text{new}} = \mathbf{I} - \tau(\mathbf{U}_m g_\psi(\Lambda_m)^{-1} \mathbf{U}_m^T - \mathbf{I})$  by Eq. (6) where  $\tau = \frac{\alpha}{1-\alpha}$  is a scaling parameter and a partial eigendecomposition [56] can be employed to produce a low-rank, robust structure for  $\hat{\mathbf{A}}^{\text{new}}$  using only  $m$  extremal eigenvalues. Equipped with this newfound graph, we proceed to perform non-local aggregation:  $\mathbf{Z}^{(l)} = (1 - \eta)\mathbf{Z}^{(0)} + \eta \hat{\mathbf{A}}^{\text{new}} \mathbf{Z}^{(l-1)}$ , where  $\eta$  refers to the update rate and  $\mathbf{Z}^{(0)} = f_\varphi(\mathbf{X})$  and  $l = 1, 2, \dots, L$  denote layer number. The iteratively aggregated results are denoted as  $\mathbf{Z}_a$ . Recognizing the potential noise from the non-local nature of  $\hat{\mathbf{A}}^{\text{new}}$ , we apply a sparsification technique, leveraging a positive threshold  $\epsilon$ , and retain only essential elements outside the  $[-\epsilon, \epsilon]$  interval. For clarity, this refined model is referred to as SAF- $\epsilon$ .

**Node-wise Prediction Amalgamation.** To leverage information from different graph domains, we employ an attention mechanism, allowing nodes to determine the importance of each space. This mechanism produces pairwise weights for a nuanced amalgamation during prediction. Specifically, the weight pair is computed as  $\kappa_f = \text{Sigmoid}(\mathcal{P}_f(\mathbf{Z}_f))$ ,  $\kappa_a = \text{Sigmoid}(\mathcal{P}_a(\mathbf{Z}_a))$  where  $\kappa_f, \kappa_a \in \mathbb{R}^N$  contain the weights for each node, and  $\mathcal{P}_f(\cdot)$  and  $\mathcal{P}_a(\cdot)$  are two different mappings from  $\mathbb{R}^C$  to  $\mathbb{R}$ . For simplicity, we implement them using two one-layer MLPs. Given domain predictions  $\mathbf{Y}_f, \mathbf{Y}_a \in \mathbb{R}^C$ , the final model prediction is attained as  $\mathbf{Y} = \text{diag}(\kappa_f) \cdot \mathbf{Y}_f + \text{diag}(\kappa_a) \cdot \mathbf{Y}_a$  where a normalization  $[\kappa_f, \kappa_a] \leftarrow \frac{[\kappa_f, \kappa_a]}{\max\{\|\kappa_f, \kappa_a\|_1, \delta\}}$  is performed beforehand to maintain  $\kappa_f + \kappa_a = \mathbf{1}$  with small value  $\delta$  preventing zero division. Similar schemes can be founded in works [57, 58, 59].

**Complexity Analysis.** SAF augments spectral GNNs with non-local aggregation and node-wise amalgamation. The first part entails creating a new graph and information propagation. In SAF- $\epsilon$ , these two steps are separated, culminating in  $\mathcal{O}(N^3 + N^2 + nnz(\hat{\mathbf{A}}^{\text{new}})d)$  complexity, where  $nnz$  denotes non-zero element count. Conversely, SAF, viewing non-local aggregation holistically, can reduce complexity to  $\mathcal{O}(2dN^2 + dN)$  when  $d \ll N$ . For node-wise amalgamation, its parallelizable nature ensures computational efficiency. Our method also requires eigendecomposition<sup>4</sup> precomputation, which, though naively complex at  $\mathcal{O}(N^3)$ , can be reduced to  $\mathcal{O}(m^2 + nnz(\hat{\mathbf{L}})m)$  using Lanczos method [56] with  $m \ll N$  iterative steps. The results are also reusable for both training and inference. We present empirical studies on both time and space overheads in Appendix F.7.

## 6 Experiments

**Datasets.** We evaluate models over 13 real-world datasets from various domains. These include three well-known homophilic graphs: Cora, Citeseer, and Pubmed [60, 61], five commonly used heterophilic graphs: Chameleon, Squirrel [62, 36], Cornell, Texas [36], and Actor [63, 36], as well as five recently introduced benchmarks: Minesweeper, Tolokers, Amazon-ratings, Roman-empire [64], and Penn94 [65, 66]. Detailed information and statistics are provided in Appendix D.

**Baselines.** We compare SAF with 21 models: (1) MLP; (2) Basic GNNs: GCN [7] and APPNP [34]; (3) Spectral GNNs: ARMA [33], GPR-GNN [9], BernNet [10], ChebNetII [12], JacobiConv [13], Specformer [39], LON-GNN [15], OptBasisGNN [16] and FLODE [40]; (4) Spatial GNNs: GCNII [22], PDE-GCN [35], NodeFormer [38], GloGNN++ [49] and LRGNN [67]; (5) Unified GNNs: GNN-LF [21], GNN-HF [21], ADA-UGNN [20] and FE-GNN [24].

**Setup.** To follow [10, 12, 13], we fix  $K = 10$ . For each dataset, we perform a grid search to tune the hyper-parameters of all models. With the best hyper-parameters, we train models with Adam optimizer [68] in 1,000 epochs using early-stopping strategy and a patience of 200 epochs, and report

<sup>4</sup>For more on its modern applications and discussions, please refer to Appendix C.2 (including baseline models Specformer [39] and FE-GNN [24] featured in our experiments) and F.7.

Table 1: Semi-supervised node classification accuracy (%)  $\pm$  95% confidence interval.

| Method               | Cham.                            | Squi.                            | Texas                            | Corn.                            | Actor                            | Cora                             | Cite.                            | Pubm.                            |
|----------------------|----------------------------------|----------------------------------|----------------------------------|----------------------------------|----------------------------------|----------------------------------|----------------------------------|----------------------------------|
| MLP                  | 26.36 $\pm$ 2.85                 | 21.42 $\pm$ 1.50                 | 32.42 $\pm$ 9.91                 | 36.53 $\pm$ 7.92                 | 29.75 $\pm$ 0.95                 | 57.17 $\pm$ 1.34                 | 56.75 $\pm$ 1.55                 | 70.52 $\pm$ 2.01                 |
| GCN                  | 38.15 $\pm$ 3.77                 | 31.18 $\pm$ 0.93                 | 34.68 $\pm$ 9.07                 | 32.36 $\pm$ 8.55                 | 22.74 $\pm$ 2.37                 | 79.19 $\pm$ 1.37                 | 69.71 $\pm$ 1.32                 | 78.81 $\pm$ 0.84                 |
| APNP                 | 32.73 $\pm$ 2.31                 | 24.50 $\pm$ 0.89                 | 34.79 $\pm$ 10.11                | 34.85 $\pm$ 9.71                 | 29.74 $\pm$ 1.04                 | 82.39 $\pm$ 0.68                 | 69.79 $\pm$ 0.92                 | 79.97 $\pm$ 1.58                 |
| ARMA                 | 37.42 $\pm$ 1.72                 | 24.15 $\pm$ 0.93                 | 39.65 $\pm$ 8.09                 | 28.90 $\pm$ 10.07                | 27.02 $\pm$ 2.31                 | 79.14 $\pm$ 1.07                 | 69.35 $\pm$ 1.44                 | 78.31 $\pm$ 1.33                 |
| GPR-GNN              | 33.03 $\pm$ 1.92                 | 24.36 $\pm$ 1.52                 | 33.98 $\pm$ 11.90                | 38.95 $\pm$ 12.36                | 28.58 $\pm$ 1.01                 | 82.37 $\pm$ 0.91                 | 69.22 $\pm$ 1.27                 | 79.28 $\pm$ 2.25                 |
| BernNet              | 27.32 $\pm$ 4.04                 | 22.37 $\pm$ 0.98                 | 43.01 $\pm$ 7.45                 | 39.42 $\pm$ 9.59                 | 29.87 $\pm$ 0.78                 | 82.17 $\pm$ 0.86                 | 69.44 $\pm$ 0.97                 | 79.48 $\pm$ 1.47                 |
| ChebNetII            | <b>43.42<math>\pm</math>3.54</b> | <b>33.96<math>\pm</math>1.22</b> | 46.58 $\pm$ 7.68                 | 42.19 $\pm$ 11.61                | 30.18 $\pm$ 0.81                 | 82.42 $\pm$ 0.64                 | 69.89 $\pm$ 1.21                 | 79.51 $\pm$ 1.03                 |
| JacobiConv           | 36.67 $\pm$ 1.63                 | 29.38 $\pm$ 0.71                 | 48.50 $\pm$ 5.90                 | 43.01 $\pm$ 11.92                | 31.69 $\pm$ 0.71                 | <u>82.93<math>\pm</math>0.55</u> | 70.25 $\pm$ 1.02                 | 79.53 $\pm$ 1.28                 |
| Specformer           | 36.05 $\pm$ 3.47                 | 29.64 $\pm$ 0.88                 | 50.00 $\pm$ 8.33                 | 43.76 $\pm$ 5.84                 | 31.45 $\pm$ 0.68                 | 81.44 $\pm$ 0.63                 | 66.11 $\pm$ 0.98                 | 78.05 $\pm$ 1.03                 |
| LON-GNN              | 35.17 $\pm$ 1.85                 | 30.25 $\pm$ 1.04                 | 45.38 $\pm$ 7.92                 | 35.32 $\pm$ 8.09                 | 31.51 $\pm$ 1.23                 | 81.93 $\pm$ 0.74                 | 70.41 $\pm$ 1.10                 | 79.57 $\pm$ 1.08                 |
| OptBasisGNN          | 35.56 $\pm$ 2.86                 | 31.25 $\pm$ 1.06                 | 37.11 $\pm$ 5.09                 | 32.31 $\pm$ 7.11                 | 31.73 $\pm$ 0.50                 | 78.69 $\pm$ 0.86                 | 63.46 $\pm$ 1.30                 | 77.38 $\pm$ 0.98                 |
| FLODE                | 40.20 $\pm$ 1.02                 | 31.99 $\pm$ 1.05                 | <u>50.29<math>\pm</math>4.74</u> | 42.89 $\pm$ 7.69                 | <u>32.18<math>\pm</math>1.10</u> | 79.90 $\pm$ 1.07                 | 69.89 $\pm$ 2.03                 | 77.78 $\pm$ 1.47                 |
| GNN-LF               | 26.49 $\pm$ 2.00                 | 22.01 $\pm$ 1.04                 | 39.02 $\pm$ 6.24                 | 36.65 $\pm$ 9.60                 | 28.28 $\pm$ 0.71                 | 81.96 $\pm$ 0.92                 | 69.80 $\pm$ 1.36                 | 79.50 $\pm$ 1.28                 |
| GNN-HF               | 35.57 $\pm$ 2.26                 | 22.36 $\pm$ 1.26                 | 44.80 $\pm$ 5.67                 | 38.79 $\pm$ 11.62                | 29.15 $\pm$ 0.78                 | 81.15 $\pm$ 0.78                 | 69.68 $\pm$ 0.73                 | 79.10 $\pm$ 1.19                 |
| ADA-UGNN             | 39.39 $\pm$ 2.02                 | 25.65 $\pm$ 0.49                 | 47.86 $\pm$ 6.65                 | 42.89 $\pm$ 8.09                 | 30.78 $\pm$ 1.00                 | 82.52 $\pm$ 1.04                 | 70.18 $\pm$ 1.40                 | 79.78 $\pm$ 1.32                 |
| FE-GNN               | 38.23 $\pm$ 1.66                 | 31.67 $\pm$ 1.60                 | 47.40 $\pm$ 5.90                 | 41.21 $\pm$ 8.96                 | 26.20 $\pm$ 0.76                 | 77.00 $\pm$ 0.74                 | 61.24 $\pm$ 1.26                 | 75.63 $\pm$ 1.33                 |
| SAF                  | 41.82 $\pm$ 1.74                 | 31.77 $\pm$ 0.69                 | 58.04 $\pm$ 3.76                 | 52.49 $\pm$ 8.56                 | 33.50 $\pm$ 0.55                 | 83.57 $\pm$ 0.66                 | 71.07 $\pm$ 1.08                 | 79.51 $\pm$ 1.12                 |
| SAF- $\epsilon$      | <u>41.88<math>\pm</math>2.04</u> | <u>32.05<math>\pm</math>0.40</u> | <b>58.38<math>\pm</math>3.47</b> | <b>53.41<math>\pm</math>5.55</b> | <b>33.84<math>\pm</math>0.58</b> | <b>83.79<math>\pm</math>0.71</b> | <b>71.30<math>\pm</math>0.93</b> | <b>80.16<math>\pm</math>1.25</b> |
| Improv. <sup>3</sup> | 14.56%                           | 9.68%                            | 15.37%                           | 13.99%                           | 3.97%                            | 1.62%                            | 1.86%                            | 0.68%                            |

the mean classification accuracies with a 95% confidence interval on 10 random data splits. More experimental details can be found in Appendix E.

**Semi-supervised Node Classification.** In this task, we follow the experimental protocol established by [12] and compare our models with MLP, two basic GNNs, eight popular polynomial spectral GNNs, and five unified GNNs. For data splitting on homophilic graphs (Cora, Citeseer, and Pubmed), we apply the standard division [69] with 20 nodes per class for training, 500 nodes for validation, and 1,000 nodes for testing. On the other five heterophilic graphs, we leverage the sparse splitting [9] with 2.5%/2.5%/95% samples respectively for training/validation/testing. The results are reported in Table 1, where the best results are bold and the underlined letters denote the second highest accuracy. We first observe that both SAF and SAF- $\epsilon$  substantially boosts its base model, BernNet, with gains reaching a notable 15.37%. This impressive enhancement is credited to their capacity to effectively exploit the task-beneficial information, which is implicitly encoded by spectral filtering in the spatial domain. This ability is particularly advantageous in contexts with limited supervision, where it allows effective leveraging of extra prior knowledge during training. Generally, our models outperform competitors on all datasets except for Chameleon and Squirrel, where SAF maintains a second-place rank with considerable improvements on BernNet by 14.56% and 9.68%. In these cases, ChebNetII initially surpasses our model, yet, with more training samples, our SAF manages to beats it by margins of 3.93% and 6.28% (see Table 2). Moreover, SAF- $\epsilon$  averagely delivers better results than SAF by using thresholding sparsity to reduce non-local noise. However, this enhancement also incurs higher computational costs, as illustrated in both Section 5 and Appendix F.7.

**Full-supervised Node Classification.** To bolster our evaluation, we expand the previously compared baselines to include five cutting-edge spatial GNN models: GCNII & PDE-GCN capturing long-range dependency, and NodeFormer, GloGNN++ & LRGNN, which go further by not only capturing long-range dependencies but also effectively addressing graph heterophily. For all datasets, we randomly divide them into 60%/20%/20% for training/validation/testing by following [10, 12]. Table 2 summarizes the mean classification accuracies. Our methods demonstrate superior performance across most datasets, with an exception on Squirrel where they achieve comparable results to Specformer. This notable performance is primarily attributed to our SAF’s effective non-local aggregation, utilizing signed edge weights to model global label relationships. This enables our methods to outperform GNNs that are specifically tailored for long-range dependency and/or graph heterophily. Besides the eight standard datasets for node classification, our study also extends to five new benchmarks [66, 64] that focus on graph heterophily. Due to space limit, we present detailed results in Appendix F.3.

**Ablation Study.** This section aims to validate our designs by comparing SAF with its three ablated variants – SAF w/o Atte., SAF w/o Spec., and SAF w/o Spat. – in full-supervised node classification. Specifically, Atte., Spec., and Spat. respectively refers to: attention mechanism in “Node-wise Prediction Amalgamation”, “Non-negative Spectral Filtering”, and “Non-local Spatial Aggregation”.

<sup>3</sup>Improv. indicates the relative improvement of our SAF over its base model, BernNet [10]. For alternative implementation using ChebNetII [12] as backbone, please refer to Appendix F.6.



Table 2: Full-supervised node classification accuracy (%)  $\pm$  95% confidence interval.

| Method               | Cham.                            | Squi.                            | Texas                            | Corn.                            | Actor                            | Cora                             | Cite.                            | Pubm.                            |
|----------------------|----------------------------------|----------------------------------|----------------------------------|----------------------------------|----------------------------------|----------------------------------|----------------------------------|----------------------------------|
| MLP                  | 46.59 $\pm$ 1.84                 | 31.01 $\pm$ 1.18                 | 86.81 $\pm$ 2.24                 | 84.15 $\pm$ 3.05                 | 40.18 $\pm$ 0.55                 | 76.89 $\pm$ 0.97                 | 76.52 $\pm$ 0.89                 | 86.14 $\pm$ 0.25                 |
| GCN                  | 60.81 $\pm$ 2.95                 | 45.87 $\pm$ 0.88                 | 76.97 $\pm$ 3.97                 | 65.78 $\pm$ 4.16                 | 33.26 $\pm$ 1.15                 | 87.18 $\pm$ 1.12                 | 79.85 $\pm$ 0.78                 | 86.79 $\pm$ 0.31                 |
| APNP                 | 52.15 $\pm$ 1.79                 | 35.71 $\pm$ 0.78                 | 90.64 $\pm$ 1.70                 | 91.52 $\pm$ 1.81                 | 39.76 $\pm$ 0.49                 | 88.16 $\pm$ 0.74                 | 80.47 $\pm$ 0.73                 | 88.13 $\pm$ 0.33                 |
| ARMA                 | 60.21 $\pm$ 1.00                 | 36.27 $\pm$ 0.62                 | 83.97 $\pm$ 3.77                 | 85.62 $\pm$ 2.13                 | 37.67 $\pm$ 0.54                 | 87.13 $\pm$ 0.80                 | 80.04 $\pm$ 0.55                 | 86.93 $\pm$ 0.24                 |
| GPR-GNN              | 67.49 $\pm$ 1.38                 | 50.43 $\pm$ 1.89                 | 92.91 $\pm$ 1.32                 | 91.57 $\pm$ 1.96                 | 39.91 $\pm$ 0.62                 | 88.54 $\pm$ 0.67                 | 80.13 $\pm$ 0.84                 | 88.46 $\pm$ 0.31                 |
| BernNet              | 68.53 $\pm$ 1.68                 | 51.39 $\pm$ 0.92                 | 92.62 $\pm$ 1.37                 | 92.13 $\pm$ 1.64                 | 41.71 $\pm$ 1.12                 | 88.51 $\pm$ 0.92                 | 80.08 $\pm$ 0.75                 | 88.51 $\pm$ 0.39                 |
| ChebNetII            | 71.37 $\pm$ 1.01                 | 57.72 $\pm$ 0.59                 | 93.28 $\pm$ 1.47                 | 92.30 $\pm$ 1.48                 | 41.75 $\pm$ 1.07                 | 88.71 $\pm$ 0.93                 | 80.53 $\pm$ 0.79                 | 88.93 $\pm$ 0.29                 |
| JacobiConv           | 74.20 $\pm$ 1.03                 | 57.38 $\pm$ 1.25                 | 93.44 $\pm$ 2.13                 | 92.95 $\pm$ 2.46                 | 41.17 $\pm$ 0.64                 | 88.98 $\pm$ 0.46                 | 80.78 $\pm$ 0.79                 | 89.62 $\pm$ 0.41                 |
| Specformer           | 75.06 $\pm$ 1.10                 | <b>65.05<math>\pm</math>0.96</b> | 90.33 $\pm$ 3.12                 | 90.00 $\pm$ 2.79                 | 42.55 $\pm$ 0.67                 | 88.85 $\pm$ 0.46                 | 80.68 $\pm$ 0.90                 | 91.25 $\pm$ 0.31                 |
| LON-GNN              | 73.00 $\pm$ 2.20                 | 60.61 $\pm$ 1.69                 | 87.54 $\pm$ 3.45                 | 84.47 $\pm$ 3.45                 | 39.10 $\pm$ 1.59                 | <u>89.44<math>\pm</math>1.12</u> | <u>81.41<math>\pm</math>1.15</u> | 90.98 $\pm$ 0.64                 |
| OptBasisGNN          | 74.26 $\pm$ 0.74                 | 63.62 $\pm$ 0.76                 | 91.15 $\pm$ 1.97                 | 89.84 $\pm$ 2.46                 | 42.39 $\pm$ 0.52                 | 87.96 $\pm$ 0.71                 | 80.58 $\pm$ 0.82                 | 90.30 $\pm$ 0.19                 |
| FLODE                | 74.38 $\pm$ 0.92                 | 63.09 $\pm$ 1.04                 | 89.34 $\pm$ 1.32                 | 89.02 $\pm$ 2.95                 | <u>42.75<math>\pm</math>1.10</u> | 88.28 $\pm$ 1.02                 | 80.66 $\pm$ 1.16                 | 90.59 $\pm$ 0.55                 |
| GCNII                | 63.44 $\pm$ 0.85                 | 41.96 $\pm$ 1.02                 | 80.46 $\pm$ 5.91                 | 84.26 $\pm$ 2.13                 | 36.89 $\pm$ 0.95                 | 88.46 $\pm$ 0.82                 | 79.97 $\pm$ 0.65                 | 89.94 $\pm$ 0.31                 |
| PDE-GCN              | 66.01 $\pm$ 1.56                 | 48.73 $\pm$ 1.06                 | 93.24 $\pm$ 2.03                 | 89.73 $\pm$ 1.35                 | 39.76 $\pm$ 0.74                 | 88.62 $\pm$ 1.03                 | 79.98 $\pm$ 0.97                 | 89.92 $\pm$ 0.38                 |
| NodeFormer           | 53.02 $\pm$ 1.58                 | 34.25 $\pm$ 1.96                 | 87.71 $\pm$ 2.13                 | 90.00 $\pm$ 3.45                 | 41.74 $\pm$ 0.61                 | 86.93 $\pm$ 1.22                 | 79.58 $\pm$ 0.85                 | <u>91.27<math>\pm</math>0.39</u> |
| GloGNN++             | 72.36 $\pm$ 0.85                 | 60.60 $\pm$ 1.04                 | 91.48 $\pm$ 1.48                 | 89.84 $\pm$ 3.62                 | 41.87 $\pm$ 1.02                 | 87.21 $\pm$ 0.59                 | 79.89 $\pm$ 0.61                 | 86.89 $\pm$ 0.33                 |
| LRGNN                | 75.01 $\pm$ 0.64                 | 63.32 $\pm$ 1.27                 | 91.80 $\pm$ 2.46                 | 90.33 $\pm$ 1.15                 | 41.16 $\pm$ 0.91                 | 88.77 $\pm$ 0.94                 | 79.85 $\pm$ 0.83                 | 90.73 $\pm$ 0.47                 |
| GNN-LF               | 53.74 $\pm$ 1.29                 | 36.15 $\pm$ 0.86                 | 76.07 $\pm$ 2.62                 | 78.36 $\pm$ 2.46                 | 38.39 $\pm$ 0.81                 | 88.51 $\pm$ 0.89                 | 79.84 $\pm$ 0.56                 | 89.86 $\pm$ 0.23                 |
| GNN-HF               | 55.97 $\pm$ 1.05                 | 35.29 $\pm$ 0.72                 | 81.15 $\pm$ 2.62                 | 85.41 $\pm$ 3.12                 | 38.96 $\pm$ 0.77                 | 88.28 $\pm$ 0.64                 | 80.04 $\pm$ 0.93                 | 90.35 $\pm$ 0.30                 |
| ADA-UGNN             | 61.09 $\pm$ 1.51                 | 42.02 $\pm$ 1.26                 | 84.92 $\pm$ 3.12                 | 83.61 $\pm$ 3.44                 | 41.10 $\pm$ 0.62                 | 88.74 $\pm$ 0.85                 | 79.81 $\pm$ 1.11                 | 90.61 $\pm$ 0.44                 |
| FE-GNN               | 73.00 $\pm$ 1.31                 | 63.28 $\pm$ 0.81                 | 88.03 $\pm$ 1.80                 | 86.07 $\pm$ 3.12                 | 41.74 $\pm$ 0.67                 | 89.21 $\pm$ 0.71                 | 80.26 $\pm$ 1.06                 | 90.80 $\pm$ 0.30                 |
| SAF                  | <b>75.30<math>\pm</math>0.96</b> | 63.63 $\pm$ 0.81                 | 94.10 $\pm$ 1.48                 | 92.95 $\pm$ 1.97                 | 42.93 $\pm$ 0.79                 | 89.80 $\pm$ 0.69                 | 80.61 $\pm$ 0.81                 | 91.49 $\pm$ 0.29                 |
| SAF- $\epsilon$      | 74.84 $\pm$ 0.99                 | <u>64.00<math>\pm</math>0.83</u> | <b>94.75<math>\pm</math>1.64</b> | <b>93.28<math>\pm</math>1.80</b> | <b>42.98<math>\pm</math>0.61</b> | <b>89.87<math>\pm</math>0.51</b> | <b>81.45<math>\pm</math>0.59</b> | <b>91.52<math>\pm</math>0.30</b> |
| Improv. <sup>3</sup> | 6.77%                            | 12.61%                           | 2.13%                            | 1.15%                            | 1.27%                            | 1.36%                            | 1.37%                            | 3.01%                            |

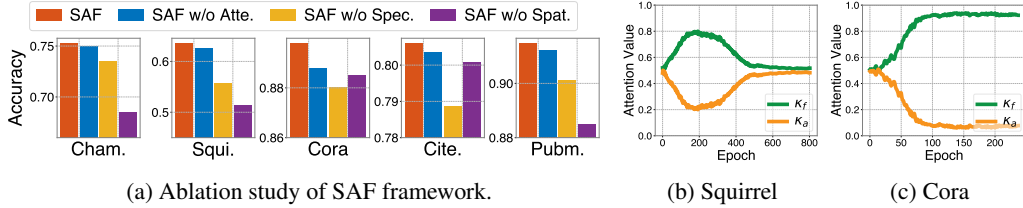


Figure 3: (a) Ablation study of SAF framework on six datasets. (b-c) Attention changing trends w.r.t. training epochs. Refer to Table 5 and Figure 6 in the Appendix for more results and visualizations.

For SAF w/o Atte., we remove the attention mechanism and equally blend predictions from different domains. SAF w/o Spec. abandons the spectral filtering phase, practically setting  $\kappa_f = 0, \kappa_a = 1$ . As the SAF w/o Spat. configuration is equivalent to BernNet model, the corresponding results are posted directly. From Figure 3(a), we can draw several insights: **1)** The impact of Atte. module on our SAF varies by datasets, e.g., on Chameleon and Squirrel, showing a slight performance reduction upon its removal. This observation aligns with our observation that their optimal attention values are close to an even split, as suggested in Figures 3(b) and 6(b). Conversely, Cora dataset exhibits a notable drop, due to its optimal attention weights being far from even, as depicted in Figure 3(c); **2)** Spectral filtering (Spec. module) remains vital for discriminative node representation learning. Specifically, the quality of the adapted new graph fundamentally hinges on the graph spectral filters' training, as underscored by their theoretical interaction in Eq. (6). Practically, the absence of spectral filtering markedly reduces model accuracy, confirming its importance in SAF; **3)** This visualization not only reaffirms the pivotal role of the non-local aggregation (Spat. module), but also underscores its position as the most crucial component in advancing spectral GNNs within the SAF framework.

**Analysis of Attention Trends.** We analyze the changing trends of the pair-wise attention weights during training SAF on Squirrel and Cora datasets. From Figure 3(b-c), the average weights for filtering and aggregation start similarly but diverge throughout training, showing different trends in heterophilic and homophilic graphs. On the heterophilic graph Squirrel, both weights converge to similar values, demonstrating their mutual importance in modeling complex connectivity. Conversely,  $\kappa_f$  becomes dominant on the homophilic graph Cora due to the sufficiency of node proximity information for label prediction, thereby diminishing the relevance of  $\kappa_a$  and non-local aggregation.

## 7 Conclusion

This paper introduces a fresh spatial perspective on spectral GNNs, shedding light on their interpretability. We reveal that spectral GNNs fundamentally leads the original graph to an adapted new one, which exhibits non-locality and accommodates signed edge weights. This insight leads to our proposed Spatially Adaptive Filtering (SAF) framework, enhancing spectral GNNs for more effective and versatile graph representation learning.

## References

- [1] Zonghan Wu, Shirui Pan, Fengwen Chen, Guodong Long, Chengqi Zhang, and Philip S. Yu. A comprehensive survey on graph neural networks. *IEEE Transactions on Neural Networks and Learning Systems*, 32(1):4–24, 2021. doi: 10.1109/TNNLS.2020.2978386.
- [2] Ines Chami, Sami Abu-El-Haija, Bryan Perozzi, Christopher Ré, and Kevin Murphy. Machine learning on graphs: A model and comprehensive taxonomy. *Journal of Machine Learning Research*, 23(89):1–64, 2022.
- [3] Chen Gao, Yu Zheng, Nian Li, Yinfeng Li, Yingrong Qin, Jinghua Piao, Yuhuan Quan, Jianxin Chang, Depeng Jin, Xiangnan He, et al. A survey of graph neural networks for recommender systems: Challenges, methods, and directions. *ACM Transactions on Recommender Systems*, 1(1):1–51, 2023.
- [4] Fan R. K. Chung. Spectral graph theory. 1996.
- [5] David I Shuman, Sunil K Narang, Pascal Frossard, Antonio Ortega, and Pierre Vandergheynst. The emerging field of signal processing on graphs: Extending high-dimensional data analysis to networks and other irregular domains. *IEEE signal processing magazine*, 30(3):83–98, 2013.
- [6] Michaël Defferrard, Xavier Bresson, and Pierre Vandergheynst. Convolutional neural networks on graphs with fast localized spectral filtering. *Advances in neural information processing systems*, 29, 2016.
- [7] Thomas N. Kipf and Max Welling. Semi-supervised classification with graph convolutional networks. In *International Conference on Learning Representations (ICLR)*, 2017.
- [8] Ron Levie, Federico Monti, Xavier Bresson, and Michael M Bronstein. Cayleynets: Graph convolutional neural networks with complex rational spectral filters. *IEEE Transactions on Signal Processing*, 67(1):97–109, 2018.
- [9] Eli Chien, Jianhao Peng, Pan Li, and Olgica Milenkovic. Adaptive universal generalized pagerank graph neural network. In *International Conference on Learning Representations*, 2021. URL <https://openreview.net/forum?id=n6jl7fLxrP>.
- [10] Mingguo He, Zhewei Wei, Hongteng Xu, et al. Bernnet: Learning arbitrary graph spectral filters via bernstein approximation. *Advances in Neural Information Processing Systems*, 34: 14239–14251, 2021.
- [11] Mingxuan Ju, Shifu Hou, Yujie Fan, Jianan Zhao, Yanfang Ye, and Liang Zhao. Adaptive kernel graph neural network. In *Proceedings of the AAAI Conference on Artificial Intelligence*, volume 36, pages 7051–7058, 2022.
- [12] Mingguo He, Zhewei Wei, and Ji-Rong Wen. Convolutional neural networks on graphs with chebyshev approximation, revisited. In *NeurIPS*, 2022.
- [13] Xiyuan Wang and Muhan Zhang. How powerful are spectral graph neural networks. In *International Conference on Machine Learning*, pages 23341–23362. PMLR, 2022.
- [14] Jingwei Guo, Kaizhu Huang, Xinping Yi, and Rui Zhang. Graph neural networks with diverse spectral filtering. In *Proceedings of the ACM Web Conference 2023*, pages 306–316, 2023.
- [15] Qian Tao, Zhen Wang, Wenyuan Yu, Yaliang Li, and Zhewei Wei. Longnn: Spectral gnns with learnable orthonormal basis. *arXiv preprint arXiv:2303.13750*, 2023.

- [16] Yuhe Guo and Zhewei Wei. Graph neural networks with learnable and optimal polynomial bases. *arXiv preprint arXiv:2302.12432*, 2023.
- [17] Muhammet Balcilar, Guillaume Renton, Pierre H  roux, Benoit Gauzere, Sebastien Adam, and Paul Honeine. Bridging the gap between spectral and spatial domains in graph neural networks. *arXiv preprint arXiv:2003.11702*, 2020.
- [18] Zhiqian Chen, Fanglan Chen, Lei Zhang, Taoran Ji, Kaiqun Fu, Liang Zhao, Feng Chen, Lingfei Wu, Charu Aggarwal, and Chang-Tien Lu. Bridging the gap between spatial and spectral domains: A unified framework for graph neural networks. *arXiv preprint arXiv:2107.10234*, 2021.
- [19] Yuhe Guo and Zhewei Wei. Clenshaw graph neural networks. In *Proceedings of the 29th ACM SIGKDD Conference on Knowledge Discovery and Data Mining*, pages 614–625, 2023.
- [20] Yao Ma, Xiaorui Liu, Tong Zhao, Yozen Liu, Jiliang Tang, and Neil Shah. A unified view on graph neural networks as graph signal denoising. In *Proceedings of the 30th ACM International Conference on Information & Knowledge Management*, pages 1202–1211, 2021.
- [21] Meiqi Zhu, Xiao Wang, Chuan Shi, Houye Ji, and Peng Cui. Interpreting and unifying graph neural networks with an optimization framework. In *Proceedings of the Web Conference 2021*, pages 1215–1226, 2021.
- [22] Ming Chen, Zhewei Wei, Zengfeng Huang, Bolin Ding, and Yaliang Li. Simple and deep graph convolutional networks. In *International conference on machine learning*, pages 1725–1735. PMLR, 2020.
- [23] Muhammet Balcilar, Renton Guillaume, Pierre H  roux, Benoit Ga  z  re, S  bastien Adam, and Paul Honeine. Analyzing the expressive power of graph neural networks in a spectral perspective. In *Proceedings of the International Conference on Learning Representations (ICLR)*, 2021.
- [24] Jiaqi Sun, Lin Zhang, Guangyi Chen, Peng Xu, Kun Zhang, and Yujiu Yang. Feature expansion for graph neural networks. In *International Conference on Machine Learning*, pages 33156–33176. PMLR, 2023.
- [25] Renjie Liao, Zhizhen Zhao, Raquel Urtasun, and Richard S Zemel. Lanczosnet: Multi-scale deep graph convolutional networks. *arXiv preprint arXiv:1901.01484*, 2019.
- [26] Werner Heisenberg.   ber den anschaulichen inhalt der quantentheoretischen kinematik und mechanik. *Zeitschrift f  r Physik*, 43(3-4):172–198, 1927.
- [27] Gerald B Folland and Alladi Sitaram. The uncertainty principle: A mathematical survey. *Journal of Fourier analysis and applications*, 3:207–238, 1997.
- [28] Ameya Agaskar and Yue M Lu. A spectral graph uncertainty principle. *IEEE Transactions on Information Theory*, 59(7):4338–4356, 2013.
- [29] Justin Gilmer, Samuel S Schoenholz, Patrick F Riley, Oriol Vinyals, and George E Dahl. Neural message passing for quantum chemistry. In *International conference on machine learning*, pages 1263–1272. PMLR, 2017.
- [30] Will Hamilton, Zhitao Ying, and Jure Leskovec. Inductive representation learning on large graphs. *Advances in neural information processing systems*, 30, 2017.
- [31] Jie Zhou, Ganqu Cui, Shengding Hu, Zhengyan Zhang, Cheng Yang, Zhiyuan Liu, Lifeng Wang, Changcheng Li, and Maosong Sun. Graph neural networks: A review of methods and applications. *AI open*, 1:57–81, 2020.
- [32] Yushun Dong, Kaize Ding, Brian Jalaian, Shuiwang Ji, and Jundong Li. Adagnn: Graph neural networks with adaptive frequency response filter. In *Proceedings of the 30th ACM International Conference on Information & Knowledge Management*, pages 392–401, 2021.

- [33] Filippo Maria Bianchi, Daniele Grattarola, Lorenzo Livi, and Cesare Alippi. Graph neural networks with convolutional arma filters. *IEEE Transactions on Pattern Analysis and Machine Intelligence*, 2021.
- [34] Johannes Gasteiger, Aleksandar Bojchevski, and Stephan Günnemann. Predict then propagate: Graph neural networks meet personalized pagerank. In *International Conference on Learning Representations (ICLR)*, 2019.
- [35] Moshe Eliasof, Eldad Haber, and Eran Treister. Pde-gcn: novel architectures for graph neural networks motivated by partial differential equations. *Advances in neural information processing systems*, 34:3836–3849, 2021.
- [36] Hongbin Pei, Bingzhe Wei, Kevin Chen-Chuan Chang, Yu Lei, and Bo Yang. Geom-gcn: Geometric graph convolutional networks. *arXiv preprint arXiv:2002.05287*, 2020.
- [37] Meng Liu, Zhengyang Wang, and Shuiwang Ji. Non-local graph neural networks. *IEEE transactions on pattern analysis and machine intelligence*, 44(12):10270–10276, 2021.
- [38] Qitian Wu, Wentao Zhao, Zenan Li, David P Wipf, and Junchi Yan. Nodeformer: A scalable graph structure learning transformer for node classification. *Advances in Neural Information Processing Systems*, 35:27387–27401, 2022.
- [39] Deyu Bo, Chuan Shi, Lele Wang, and Renjie Liao. Specformer: Spectral graph neural networks meet transformers. *arXiv preprint arXiv:2303.01028*, 2023.
- [40] Sohir Maskey, Raffaele Paolino, Aras Bacho, and Gitta Kutyniok. A fractional graph laplacian approach to oversmoothing. *Advances in Neural Information Processing Systems*, 36, 2023.
- [41] Michele Benzi, Daniele Bertaccini, Fabio Durastante, and Igor Simunec. Non-local network dynamics via fractional graph laplacians. *Journal of Complex Networks*, 8(3):cnaa017, 2020.
- [42] Jiong Zhu, Yujun Yan, Lingxiao Zhao, Mark Heimann, Leman Akoglu, and Danai Koutra. Beyond homophily in graph neural networks: Current limitations and effective designs. *Advances in Neural Information Processing Systems*, 33:7793–7804, 2020.
- [43] Miller McPherson, Lynn Smith-Lovin, and James M Cook. Birds of a feather: Homophily in social networks. *Annual review of sociology*, 27(1):415–444, 2001.
- [44] Deyu Bo, Xiao Wang, Chuan Shi, and Huawei Shen. Beyond low-frequency information in graph convolutional networks. In *Proceedings of the AAAI Conference on Artificial Intelligence*, volume 35, pages 3950–3957, 2021.
- [45] Ruijia Wang, Shuai Mou, Xiao Wang, Wanpeng Xiao, Qi Ju, Chuan Shi, and Xing Xie. Graph structure estimation neural networks. In *Proceedings of the Web Conference 2021*, pages 342–353, 2021.
- [46] Yuchen Yan, Yuzhong Chen, Huiyuan Chen, Minghua Xu, Mahashweta Das, Hao Yang, and Hanghang Tong. From trainable negative depth to edge heterophily in graphs. In *Thirty-seventh Conference on Neural Information Processing Systems*, 2023.
- [47] Jaemin Yoo, Meng-Chieh Lee, Shubhanshu Shekhar, and Christos Faloutsos. Less is more: Slim for accurate, robust, and interpretable graph mining. In *Proceedings of the 29th ACM SIGKDD Conference on Knowledge Discovery and Data Mining*, pages 3128–3139, 2023.
- [48] Guanyu Cui and Zhewei Wei. Mgnn: Graph neural networks inspired by distance geometry problem. In *Proceedings of the 29th ACM SIGKDD Conference on Knowledge Discovery and Data Mining*, pages 335–347, 2023.
- [49] Xiang Li, Renyu Zhu, Yao Cheng, Caihua Shan, Siqiang Luo, Dongsheng Li, and Weining Qian. Finding global homophily in graph neural networks when meeting heterophily. In *International Conference on Machine Learning*, pages 13242–13256. PMLR, 2022.
- [50] Langzhang Liang, Xiangjing Hu, Zenglin Xu, Zixing Song, and Irwin King. Predicting global label relationship matrix for graph neural networks under heterophily. In *Thirty-seventh Conference on Neural Information Processing Systems*, 2023.

- [51] Daniel Spielman. Spectral graph theory. *Combinatorial scientific computing*, 18:18, 2012.
- [52] Roger A Horn and Charles R Johnson. *Matrix analysis*. Cambridge university press, 2012.
- [53] Rida T Farouki. The bernstein polynomial basis: A centennial retrospective. *Computer Aided Geometric Design*, 29(6):379–419, 2012.
- [54] Victoria Powers and Bruce Reznick. Polynomials that are positive on an interval. *Transactions of the American Mathematical Society*, 352(10):4677–4692, 2000.
- [55] David K Hammond, Pierre Vandergheynst, and Rémi Gribonval. Wavelets on graphs via spectral graph theory. *Applied and Computational Harmonic Analysis*, 30(2):129–150, 2011.
- [56] Cornelius Lanczos. An iteration method for the solution of the eigenvalue problem of linear differential and integral operators. 1950.
- [57] Omer Sagi and Lior Rokach. Ensemble learning: A survey. *Wiley Interdisciplinary Reviews: Data Mining and Knowledge Discovery*, 8(4):e1249, 2018.
- [58] Xiao Wang, Meiqi Zhu, Deyu Bo, Peng Cui, Chuan Shi, and Jian Pei. Am-gcn: Adaptive multi-channel graph convolutional networks. In *Proceedings of the 26th ACM SIGKDD International conference on knowledge discovery & data mining*, pages 1243–1253, 2020.
- [59] Shichao Zhu, Shirui Pan, Chuan Zhou, Jia Wu, Yanan Cao, and Bin Wang. Graph geometry interaction learning. *Advances in Neural Information Processing Systems*, 33:7548–7558, 2020.
- [60] Prithviraj Sen, Galileo Namata, Mustafa Bilgic, Lise Getoor, Brian Galligher, and Tina Eliassi-Rad. Collective classification in network data. *AI magazine*, 29(3):93–93, 2008.
- [61] Galileo Namata, Ben London, Lise Getoor, Bert Huang, and U Edu. Query-driven active surveying for collective classification. In *10th international workshop on mining and learning with graphs*, volume 8, page 1, 2012.
- [62] Benedek Rozemberczki, Carl Allen, and Rik Sarkar. Multi-scale attributed node embedding. *Journal of Complex Networks*, 9(2):cnab014, 2021.
- [63] Jie Tang, Jimeng Sun, Chi Wang, and Zi Yang. Social influence analysis in large-scale networks. In *Proceedings of the 15th ACM SIGKDD international conference on Knowledge discovery and data mining*, pages 807–816, 2009.
- [64] Oleg Platonov, Denis Kuznedelev, Michael Diskin, Artem Babenko, and Liudmila Prokhorenkova. A critical look at the evaluation of gnns under heterophily: are we really making progress? *arXiv preprint arXiv:2302.11640*, 2023.
- [65] Amanda L Traud, Peter J Mucha, and Mason A Porter. Social structure of facebook networks. *Physica A: Statistical Mechanics and its Applications*, 391(16):4165–4180, 2012.
- [66] Derek Lim, Felix Hohne, Xiuyu Li, Sijia Linda Huang, Vaishnavi Gupta, Omkar Bhalerao, and Ser Nam Lim. Large scale learning on non-homophilous graphs: New benchmarks and strong simple methods. *Advances in Neural Information Processing Systems*, 34:20887–20902, 2021.
- [67] Langzhang Liang, Xiangjing Hu, Zenglin Xu, Zixing Song, and Irwin King. Predicting global label relationship matrix for graph neural networks under heterophily. *Advances in Neural Information Processing Systems*, 36, 2023.
- [68] Diederik P Kingma and Jimmy Ba. Adam: A method for stochastic optimization. *arXiv preprint arXiv:1412.6980*, 2014.
- [69] Zhilin Yang, William Cohen, and Ruslan Salakhudinov. Revisiting semi-supervised learning with graph embeddings. In *International conference on machine learning*, pages 40–48. PMLR, 2016.
- [70] Yunfeng Cai, Guanhua Fang, and Ping Li. A note on sparse generalized eigenvalue problem. *Advances in Neural Information Processing Systems*, 34:23036–23048, 2021.

- [71] Mikhail Belkin and Partha Niyogi. Laplacian eigenmaps for dimensionality reduction and data representation. *Neural computation*, 15(6):1373–1396, 2003.
- [72] Vijay Prakash Dwivedi, Chaitanya K Joshi, Anh Tuan Luu, Thomas Laurent, Yoshua Bengio, and Xavier Bresson. Benchmarking graph neural networks. *arXiv preprint arXiv:2003.00982*, 2020.
- [73] Yuning You, Tianlong Chen, Zhangyang Wang, and Yang Shen. Graph domain adaptation via theory-grounded spectral regularization. In *The Eleventh International Conference on Learning Representations*, 2022.
- [74] Heng Chang, Yu Rong, Tingyang Xu, Yatao Bian, Shiji Zhou, Xin Wang, Junzhou Huang, and Wenwu Zhu. Not all low-pass filters are robust in graph convolutional networks. *Advances in Neural Information Processing Systems*, 34:25058–25071, 2021.
- [75] Haorui Wang, Haoteng Yin, Muhan Zhang, and Pan Li. Equivariant and stable positional encoding for more powerful graph neural networks. In *International Conference on Learning Representations*, 2022.
- [76] Devin Kreuzer, Dominique Beaini, Will Hamilton, Vincent Létourneau, and Prudencio Tossou. Rethinking graph transformers with spectral attention. *Advances in Neural Information Processing Systems*, 34:21618–21629, 2021.
- [77] Jinwoo Kim, Dat Nguyen, Seonwoo Min, Sungjun Cho, Moontae Lee, Honglak Lee, and Seunghoon Hong. Pure transformers are powerful graph learners. *Advances in Neural Information Processing Systems*, 35:14582–14595, 2022.
- [78] Ladislav Rampášek, Michael Galkin, Vijay Prakash Dwivedi, Anh Tuan Luu, Guy Wolf, and Dominique Beaini. Recipe for a general, powerful, scalable graph transformer. *Advances in Neural Information Processing Systems*, 35:14501–14515, 2022.
- [79] Derek Lim, Joshua Robinson, Lingxiao Zhao, Tess Smidt, Suvrit Sra, Haggai Maron, and Stefanie Jegelka. Sign and basis invariant networks for spectral graph representation learning. *arXiv preprint arXiv:2202.13013*, 2022.
- [80] Derek Lim, Joshua Robinson, Stefanie Jegelka, and Haggai Maron. Expressive sign equivariant networks for spectral geometric learning. *arXiv preprint arXiv:2312.02339*, 2023.
- [81] Oleg Platonov, Denis Kuznedelev, Artem Babenko, and Liudmila Prokhorenkova. Characterizing graph datasets for node classification: Homophily-heterophily dichotomy and beyond. In *The Second Learning on Graphs Conference*, 2023.
- [82] Adam Paszke, Sam Gross, Francisco Massa, Adam Lerer, James Bradbury, Gregory Chanan, Trevor Killeen, Zeming Lin, Natalia Gimelshein, Luca Antiga, et al. Pytorch: An imperative style, high-performance deep learning library. *Advances in neural information processing systems*, 32, 2019.
- [83] Matthias Fey and Jan E. Lenssen. Fast graph representation learning with PyTorch Geometric. In *ICLR Workshop on Representation Learning on Graphs and Manifolds*, 2019.
- [84] Matthias Fey and Jan E. Lenssen. Fast graph representation learning with PyTorch Geometric. In *ICLR Workshop on Representation Learning on Graphs and Manifolds*, 2019.
- [85] Takuya Akiba, Shotaro Sano, Toshihiko Yanase, Takeru Ohta, and Masanori Koyama. Optuna: A next-generation hyperparameter optimization framework. In *Proceedings of the 25th ACM SIGKDD international conference on knowledge discovery & data mining*, pages 2623–2631, 2019.

## A Overall Pipeline of Spatially Adaptive Filtering Framework

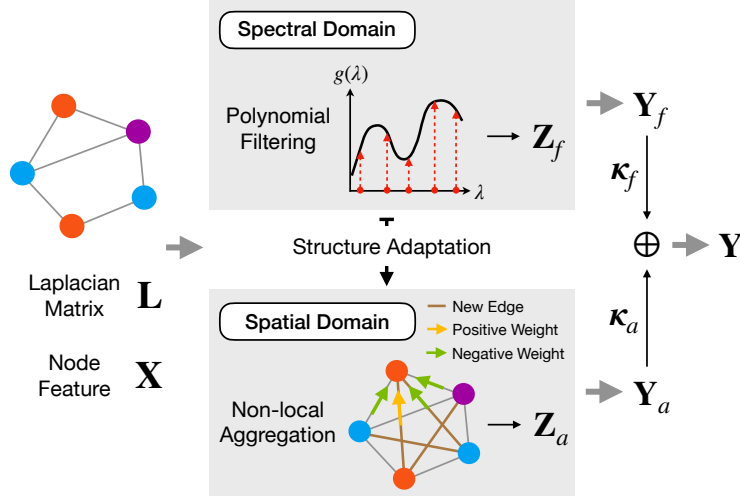


Figure 4: Illustration of SAF framework where varying node colors represent different node labels. SAF leverages the adapted new graph by spectral filtering for auxiliary non-local aggregation in the spatial domain and allows individual nodes to flexibly balance between spectral and spatial features.

## B Proofs

### B.1 Proof of Proposition 1

*Proof.* We begin with the assertion that the eigenvalues of  $\mathbf{I} - g_\psi(\hat{\mathbf{L}})$  are positive and strictly less than 1, which fulfills the necessary condition for the Neumann series expansion stated in Lemma 1. As such, we can deduce  $g_\psi(\hat{\mathbf{L}})^{-1} = (\mathbf{I} - (\mathbf{I} - g_\psi(\hat{\mathbf{L}})))^{-1} = \sum_{t=0}^{\infty} (\mathbf{I} - g_\psi(\hat{\mathbf{L}}))^t$ . Owing to the prevalent polynomial approximation, we are eligible to express  $g_\psi(\hat{\mathbf{L}})$  w.r.t. adjacency matrix  $\hat{\mathbf{A}}$ , i.e.,  $g_\psi(\hat{\mathbf{L}}) = g_\psi(\mathbf{I} - \hat{\mathbf{A}}) = \sum_{k=0}^K \pi_k \hat{\mathbf{A}}^k$  where  $\pi_k$  refers to the new coefficients made up of  $\{\psi_m\}_{m=0}^K$ . Substituting this polynomial representation into our Neumann expansion, we obtain  $g_\psi(\hat{\mathbf{L}})^{-1} = \sum_{n=0}^{\infty} (\mathbf{I} - \sum_{k=0}^K \pi_k \hat{\mathbf{A}}^k)^n$ . Now, revisiting  $\hat{\mathbf{A}}^{\text{new}}$  in Eq. (6), we have  $\hat{\mathbf{A}}^{\text{new}} = \mathbf{I} - \frac{\alpha}{1-\alpha} (g_\psi(\hat{\mathbf{L}})^{-1} - \mathbf{I}) = \mathbf{I} - \frac{\alpha}{1-\alpha} \sum_{t=1}^{\infty} (\mathbf{I} - \sum_{k=0}^K \pi_k \hat{\mathbf{A}}^k)^t = \sum_{t=0}^{\infty} \phi_t \hat{\mathbf{A}}^t$  where  $\phi_t$  is a constant coefficient made up of  $\{\pi_m\}_{m=0}^K$ .  $\square$

### B.2 Proof of Proposition 2

*Proof.* Let us commence the proof by contradiction. Let  $\mathcal{C}$  denote the condition described in proposition 2. Assume, for the sake of contradiction, that  $\mathcal{C}$  is not requisite for the optimal node representations  $\mathbf{Z}^*$  to be predictive of node labels. Under this assumption, there are node pairs  $v_i, v_j \in \mathcal{V}$  such that: (1) if  $\mathbf{y}_i = \mathbf{y}_j$ ,  $\hat{A}_{i,j}^{\text{new}} < 0$ ; (2) if  $\mathbf{y}_i \neq \mathbf{y}_j$ ,  $\hat{A}_{i,j}^{\text{new}} > 0$ . Without loss of generality, given the non-locality as proved in proposition 1, we exclude cases where  $\hat{A}_{i,j}^{\text{new}} = 0$  from our consideration. Now, consider the second objective term  $\text{tr}(\mathbf{Z}^T \gamma_\theta(\hat{\mathbf{L}}) \mathbf{Z})$  in Eq. (3). Using the relationship  $\gamma_\theta(\hat{\mathbf{L}}) = \mathbf{I} - \hat{\mathbf{A}}^{\text{new}}$ , we can expand this term into  $\sum_{v_i, v_j \in \mathcal{V}} \hat{A}_{i,j}^{\text{new}} \|\mathbf{Z}_i - \mathbf{Z}_j\|_2^2$ . Under (1), for same-class nodes  $v_i, v_j$  with  $\hat{A}_{i,j}^{\text{new}} < 0$ , minimizing the objective term pulls  $\mathbf{Z}_i$  and  $\mathbf{Z}_j$  apart in the latent space. This behavior violates the canonical understanding that nodes from the same class should exhibit similar representations. Under (2), for different-class nodes  $v_i, v_j$  with  $\hat{A}_{i,j}^{\text{new}} > 0$ , the optimization encourages  $\mathbf{Z}_i$  and  $\mathbf{Z}_j$  to be more similar. This is in direct opposition to the basic classification principle that nodes from different classes should have distinct representations. Given these contradictions stemming from the mathematical implications in optimization, we must reject assumptions (1) and (2), affirming the necessary condition  $\mathcal{C}$  for accurate label prediction by  $\mathbf{Z}^*$ .  $\square$

### B.3 Proof of Proposition 3

*Proof.* We denote  $p(x) = \sum_{k=0}^K \psi_k \binom{K}{k} (1-x)^{K-k} x^k$  as a Bernstein polynomial with  $\psi_k \geq 0$  for all  $k$  and  $\psi_{\max} = \max\{\psi_k\}_{k=0}^K$ . Given  $x \in [0, 1]$ , we can derive the following inequality as

$$\begin{aligned} p(x) &= \sum_{k=0}^K \psi_k \binom{K}{k} (1-x)^{K-k} x^k \leq \psi_{\max} \sum_{k=0}^K \binom{K}{k} (1-x)^{K-k} x^k \\ &= \psi_{\max} (1-x+x)^K = \psi_{\max}. \end{aligned}$$

Therefore, we have  $p(x) \leq \max\{\psi_k\}_{k=0}^K$  for all  $x \in [0, 1]$ .  $\square$

## C Future Remarks about Related Works

### C.1 Polynomial Spectral Graph Neural Networks

**Vanilla GCN [7].** The vanilla GCN truncates Chebyshev polynomials to a simple first-order for efficient graph convolution, which functions as a low-pass filter, i.e.,  $\mathbf{Z} = w(\mathbf{I} + \mathbf{D}^{-\frac{1}{2}} \mathbf{A} \mathbf{D}^{-\frac{1}{2}}) \mathbf{X}$ . To ensure numerical stability, it further leverages a renormalization trick to replace  $\mathbf{I} + \mathbf{D}^{-\frac{1}{2}} \mathbf{A} \mathbf{D}^{-\frac{1}{2}}$  with  $(\mathbf{D} + \mathbf{I})^{-\frac{1}{2}} (\mathbf{A} + \mathbf{I}) (\mathbf{D} + \mathbf{I})^{-\frac{1}{2}}$  and derives each graph convolution layer as

$$\mathbf{Z}^{(k+1)} = \tilde{\mathbf{D}}^{-\frac{1}{2}} \tilde{\mathbf{A}} \tilde{\mathbf{D}}^{-\frac{1}{2}} \mathbf{Z}^{(k)} \mathbf{W}^{(k)},$$

where  $\tilde{\mathbf{A}} = \mathbf{A} + \mathbf{I}$ ,  $\tilde{\mathbf{D}} = \mathbf{D} + \mathbf{I}$ ,  $\mathbf{Z}^{(0)} = \mathbf{X}$ , and  $\mathbf{W}^{(k)}$  denotes learnable weights in the  $k$ -th layer.

**GPR-GNN [9].** GPR-GNN leverages the Generalized PageRank to approximate spectral graph filters with Monomial polynomial basis. The model architecture is formulated as

$$\mathbf{Z} = \sum_{k=0}^K \psi_k \hat{\mathbf{A}}^k f_{\varphi}(\mathbf{X}),$$

where  $\hat{\mathbf{A}} = \tilde{\mathbf{D}}^{\frac{1}{2}} \tilde{\mathbf{A}} \tilde{\mathbf{D}}^{\frac{1}{2}}$ , and  $f_{\varphi}(\mathbf{X})$  refers to a linear map with parameters  $\varphi$ . The approximated graph filter is  $g_{\psi}(\tilde{\lambda}) = \sum_{k=0}^K \psi_k \tilde{\lambda}^k$  with  $\tilde{\lambda}$  being the eigenvalues of  $\hat{\mathbf{A}}$ .

**BernNet [10].** BernNet approximates graph filters with Bernstein polynomials to attain non-negative property, yielding the model expression as

$$\mathbf{Z} = \sum_{k=0}^K \psi_k \frac{1}{2^K} \binom{K}{k} (2\mathbf{I} - \hat{\mathbf{L}})^{K-k} \hat{\mathbf{L}}^k f_{\varphi}(\mathbf{X}).$$

The graph filter is defined as  $g_{\psi}(\lambda) = \sum_{k=0}^K \psi_k \frac{1}{2^K} \binom{K}{k} (2 - \lambda)^{K-k} \lambda^k$  and  $\lambda$  is the eigenvalue of  $\hat{\mathbf{L}}$ .

**ChebNetII [12].** ChebNetII leverages Chebyshev interpolation to approximate graph filter while reducing the Runge phenomenon. This results in the following model structure:

$$\mathbf{Z} = \mathbf{Y} = \frac{2}{K+1} \sum_{k=0}^K \sum_{j=0}^K \gamma_j T_k(x_j) T_k(\hat{\mathbf{L}}) f_{\varphi}(\mathbf{X}).$$

Here,  $T_k(x) = 2xT_{k-1}(x) - T_{k-2}(x)$  denotes the Chebyshev basis with  $T_0(x) = 1$  and  $T_1(x) = x$ , and  $x_j = \cos(\frac{(j+1/2)\pi}{K+1})$  refers to the Chebyshev nodes of  $T_{K+1}(x)(\cdot)$ . The graph filter corresponds to  $g_{\psi}(\lambda) = \frac{2}{K+1} \sum_{k=0}^K \psi_k T_k(\lambda)$  with  $\psi_k = \sum_{j=0}^K \gamma_j T_k(x_j)$ .

Despite the proliferation of various filtering strategies, they invariably resort to approximating graph filters with fixed-order polynomials. While this approach does offer computational advantages, the truncated approximation limits the effective propagation range and hinder the ability to capture the long-range dependencies.



Table 3: Statistics of real-world datasets.  $F$  and  $C$  denotes the number of features and classes.  $\Delta$  represents graph diameter referring to the longest geodesic distance between nodes on the graph. For Penn94, due to multiple subgraphs, we report  $\Delta$  of the largest connected component.

| Dataset        | $ \mathcal{V} $ | $ \mathcal{E} $ | $F$   | $C$ | $\Delta$ | $\mathcal{H}$ | $\mathcal{H}_{\text{class}}$ | $\mathcal{H}_{\text{adjusted}}$ |
|----------------|-----------------|-----------------|-------|-----|----------|---------------|------------------------------|---------------------------------|
| Chameleon      | 2,227           | 36,101          | 2,325 | 5   | 11       | 0.23          | 0.06                         | 0.03                            |
| Squirrel       | 5,201           | 217,073         | 2,089 | 5   | 10       | 0.22          | 0.03                         | 0.01                            |
| Texas          | 183             | 309             | 1,703 | 5   | 8        | 0.11          | 0.00                         | -0.23                           |
| Cornell        | 183             | 295             | 1,703 | 5   | 8        | 0.30          | 0.05                         | -0.08                           |
| Actor          | 7,600           | 33,544          | 931   | 5   | 12       | 0.22          | 0.01                         | 0.00                            |
| Cora           | 2,708           | 5,429           | 1,433 | 7   | 19       | 0.81          | 0.77                         | 0.77                            |
| Citeseer       | 3,327           | 4,732           | 3,703 | 6   | 28       | 0.74          | 0.63                         | 0.67                            |
| Pubmed         | 19,717          | 44,338          | 500   | 3   | 18       | 0.80          | 0.66                         | 0.69                            |
| Minesweeper    | 10,000          | 39,402          | 7     | 2   | 99       | 0.68          | 0.01                         | 0.01                            |
| Tolokers       | 11,758          | 519,000         | 10    | 2   | 11       | 0.59          | 0.18                         | 0.09                            |
| Amazon-ratings | 24,492          | 93,050          | 300   | 5   | 46       | 0.38          | 0.13                         | 0.14                            |
| Roman-empire   | 22,662          | 32,927          | 300   | 18  | 6,824    | 0.05          | 0.02                         | -0.05                           |
| Penn94         | 41,554          | 1,362,229       | 5     | 2   | 8        | 0.47          | 0.05                         | 0.02                            |

## C.2 Practical Implications of Eigendecomposition

Eigendecomposition breaks down a matrix into its eigenvalues and eigenvectors, offering insights into matrix properties, especially for the graph Laplacian. Despite computational demands, this technique has attracted surging interest in the graph learning community due to its theoretical richness, and it can be practically expedited for larger graphs using Lanczos [56] and Sparse Generalized Eigenvalue [70] algorithms. Recent advancements also underscore its value in various applications such as graph positional encoding [71, 72], spectral graph convolution [25], graph domain adaptation [73], and graph robustness [74]. For example, Laplacian eigenvectors have been widely used in identifying global position of nodes in the graph [75], particularly in recent popular graph transformers [76, 77, 78], enhancing their expressiveness. Innovations like SignNet, BasisNet [79], and Sign Equivariant [80] have further optimized the processing of these eigenvectors. When exploring the expressive power of GNN models, Specformer [39] employs eigendecomposition for learning set-to-set graph filters, TEDGCN [46] leverages it for adaptive weighting of eigengraphs, and FE-GNN [24] taps into singular value decomposition (SVD) for graph feature expansion. In line with these developments, our method, SAF, also utilizes eigendecomposition to explicitly create a new graph, enabling efficient non-local aggregation with signed weights to tackle long-range dependency and graph heterophily.

## D Dataset Information

We conduct experiments on 13 real-world datasets from various domains. The detailed data statistics are summarized in Table 3. Alongside standard data attributes, we also provide the longest geodesic (shortest-path) distance between graph nodes for better illustrating the non-local property that we investigate in Figures 1 and 5. Moreover, we adopt three metrics - edge homophily [42]  $\mathcal{H}$ , class homophily [66]  $\mathcal{H}_{\text{class}}$ , and adjusted homophily [81]  $\mathcal{H}_{\text{adjusted}}$  - to assess the graph’s homophily ratio, which ranges from 0 (high heterophily) to 1 (high homophily). While the first is a commonly used index, the latter two, considering class variability and potential imbalance, have been recently introduced for more accurate estimation. For our main text analysis regarding the adapted new graph, we primarily rely on the edge homophily metric, defined as  $\mathcal{H} = |\{(v_i, v_j) | (v_i, v_j) \in \mathcal{E} \wedge \mathbf{y}_i = \mathbf{y}_j\}| / |\mathcal{E}|$ , given its simplicity and wide usage. In certain compact sections of this paper, we use four-letter abbreviations for dataset names.

- **Chameleon and Squirrel** are two Wikipedia networks collected by [62] where web pages are connected by mutual links. For the classification task, we utilize the class labels provided by [36], categorizing nodes into 5 classes according to the number of their average monthly traffic.
- **Texas and Cornell** are two webpage datasets collected by CMU WebKB project<sup>5</sup>, where nodes are web pages classified into five categories (student, project, course, staff, and faculty) and edges denote hyperlinks between them. In this study, we use the preprocessed version by [36].

<sup>5</sup><https://www.cs.cmu.edu/afs/cs.cmu.edu/project/theo-11/www/wwkb/>

- **Actor** is an actor co-occurrence network induced from the film-director-actor-writer network [63] by [36]. In this network, nodes are actors categorized into five classes, and edges correspond to their co-occurrence in Wikipedia pages.
- **Cora, Citeseer, and Pubmed** are three widely used citation network benchmark datasets [60, 61], where nodes are scientific papers and edges denote undirected citations. Each node is assigned with one class label based on its research topic as well as bag-of-word features.
- **Minesweeper, Tolokers, Amazon-ratings, and Roman-empire** are recently proposed benchmarks by [64] (with MIT license) for specifically evaluating GNN models under heterophily setting.
- **Penn94** is a large-scale friendship network [65] from the Facebook 100 networks, where nodes denote students that are labeled with reported genders and posses features such as major, second major/minor, dorm/house, year, and high school. This work uses the version preprocessed by [66].

## E Experimental Details

In this section, we provide experimental details for reproducibility. As He et al. [12] have made a comprehensive evaluation and share the same experimental protocol with us, we directly leverage their results for models: MLP, GCN, APPNP, ARMA, GPR-GNN, BernNet, ChebNetII, GCNII and PDE-GCN on datasets including Chameleon, Squirrel, Texas, Cornell, Actor, Cora, Citeseer, and Pubmed. For JacobiConv, LON-GNN, and OptBasisGNN, we also report their results from corresponding papers [13, 15, 16]. For other experiments, we utilize publicly available codes for baselines (see Appendix E.1) and implement our methods using PyTorch [82] (3-clause BSD license) and PyTorch-Geometric library [83] (MIT license) for graph representation learning. All experiments are conducted on a machine equipped with an NVIDIA GeForce RTX 3090 (24GB) and an Intel(R) Xeon(R) Gold 5218R CPU @ 2.10GHz (20 cores).

### E.1 Baseline Implementations

In our experiments, we leverage the Pytorch Geometric library [84] implementations for GCN and APPNP. For MLP, we include a sequence of linear layers, each of which is followed by batch normalization, ReLU activation, and dropout. The number of MLP layers are tuned from 1 to 5. For the remaining baselines, we use their publicly released code. Besides, for the work [49], only the most effective model variant, GloGNN++, is included in our experiments. Models like Geom-GCN [36] and Non-Local GNNs [37], surpassed by these SOTA methods, are excluded from our comparison.

- Pytorch Geometric Library: [https://github.com/pyg-team/pytorch\\_geometric](https://github.com/pyg-team/pytorch_geometric)
- GPR-GNN: <https://github.com/jianhao2016/GPRGNN>
- BernNet: <https://github.com/ivam-he/BernNet>
- ChebNetII: <https://github.com/ivam-he/ChebNetII>
- JacobiConv: <https://github.com/GraphPKU/JacobiConv>
- Specformer: <https://github.com/DSL-Lab/Specformer>
- LON-GNN: <https://github.com/TaoLbr1993/LON-GNN>
- OptBasisGNN: <https://github.com/yuziGuo/FarOptBasis>
- FLODE: <https://github.com/rpaolino/flode>
- NoderFormer: <https://github.com/qitianwu/NodeFormer>
- GloGNN++: <https://github.com/RecklessRonan/GloGNN>
- LRGNN: <https://github.com/Jinx-byebye/LRGNN>
- GNN-LF/HF: <https://github.com/zhumeiqiBUPT/GNN-LF-HF>
- ADA-UGNN: <https://github.com/alge24/ADA-UGNN>
- FE-GNN: <https://github.com/sajqavril/Feature-Extension-Graph-Neural-Networks>

### E.2 Our Implementations

The main codes for our proposed SAF can be founded in the supplementary material.

### E.3 Hyper-parameters Setting

We perform a grid search on the hyper-parameters of all models (including baselines) for each dataset using the open-source package Optuna [85]. To accommodate extensive experiments across diverse datasets in both semi- and full-supervised setting, we define a broad searching space as: learning rate  $\text{lr} \sim \{1\text{e-}3, 5\text{e-}3, 1\text{e-}2, 5\text{e-}2, 0.1\}$ , weight decay  $\text{L}_2 \sim \{0.0, 1\text{e-}6, 5\text{e-}6, 1\text{e-}5, 5\text{e-}5, 1\text{e-}4, 5\text{e-}4, 1\text{e-}3, 5\text{e-}3, 1\text{e-}2\}$ , dropout  $\sim \{0.0, 0.1, \dots, 0.8\}$  with step 0.1, non-local aggregation step  $L \sim \{1, 2, \dots, 10\}$  with step 1, scaling parameter  $\tau \sim \{0.1, 0.2, \dots, 1.0\}$  with step 0.1, update rate  $\eta \sim \{0.1, 0.2, \dots, 1.0\}$  with step 0.1, and threshold  $\epsilon \sim \{0.0, 1\text{e-}5, 5\text{e-}5, 1\text{e-}4, 5\text{e-}4, 1\text{e-}3, 5\text{e-}3, 1\text{e-}2\}$ . For other parameters specific to different base models, we strictly follow their instructions in the original papers.

## F More Experiments

### F.1 Empirical Evidence of the New Graph & Attention Trends

Additional empirical support for the newfound graph’s properties is presented in Figures 5 and 6(a). For the analysis of attention trends while training our SAF, we provide visualizations on more datasets in Figure 6(b-c). It is noteworthy that, despite Pubmed being a homophilic graph with  $\mathcal{H} = 0.80$ , non-local aggregation maintains a pivotal role in our SAF, diverging from the patterns observed on the Cora dataset as shown in Figure 3(c) of the main text. This discrepancy owes much to the sizable node count within Pubmed, where the capability of non-local aggregation in capturing long-range dependencies proves advantageous for improving model performance.

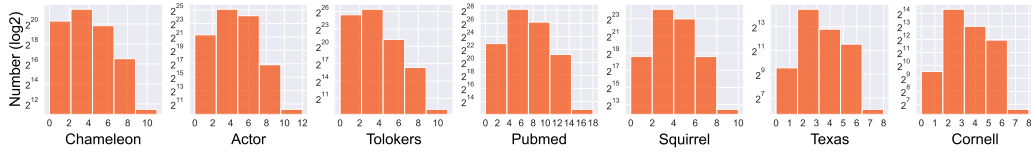
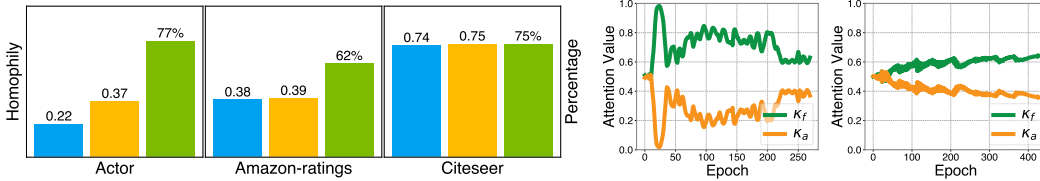


Figure 5: Distributions of original hop distance between adjacent nodes in the adapted new graph on additional seven datasets. The number of bins is set as five for better histogram visualization.



(a) The property of the newfound graph’s signed edge weights.

(b) Chameleon

(c) Pubmed

Figure 6: (a) Additional visualizations where blue, yellow, and green bars share the same meanings as in the main text (see Figure 2). (b-c) Additional attention changing trends w.r.t. training epochs.

### F.2 Empirical Verification of Supervision Dependence in GloGNN++ and LRGNN

This subsection empirically verifies the heavy reliance on label supervision for both GloGNN++ [49] and LRGNN [67] models. In Figure 7, we compare the improved classification accuracy of these models and our SAF upon the vanilla GCN under a semi-supervised setting. The figure illustrates that, despite competitive results under dense supervision (Table 2), the performance of both GloGNN++ and LRGNN deteriorates, showing negative optimization on many datasets, when the label rate drops approximately from 60% to 2.5%. This degradation highlights their dependency on high label rates for effective learning. In contrast, our SAF consistently delivers good performance regardless of the supervision level, demonstrating its effectiveness in both high and low label rate scenarios.

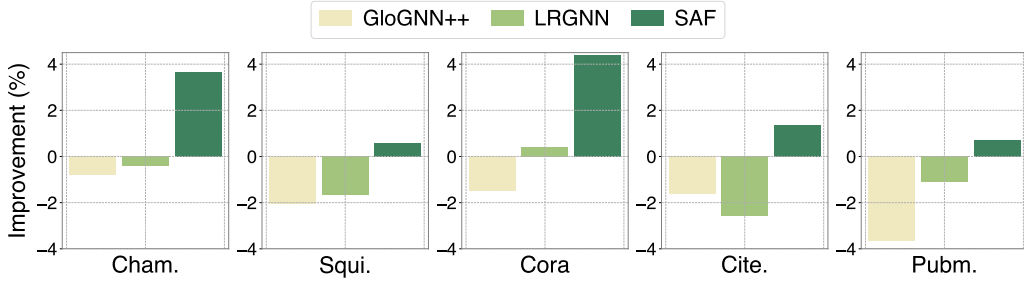


Figure 7: Improved classification accuracy by GloGNN++, LRGNN and SAF upon the vanilla GCN under semi-supervised setting (approximately 2.5%/2.5%/95% for training/validation/testing).

### F.3 New Benchmarks for Graph Heterophily

For a more extensive evaluation across various domains, we also test SAF on five recently introduced datasets, including Mine., Tolo., Amaz., Roma., and Penn94 [64, 66]. In this context, we draw comparisons solely with MLP, GCN, APPNP, along with seven GNN models that have previously shown promising results in prior tasks, namely GPR-GNN, BernNet, ChebNetII, JacobiConv, NodeFormer, GloGNN++ and FE-GNN. Table 4 lists the average classification accuracies, obtained over random splits provided by [64, 66], with a distribution of 50%/25%/25% for training/validation/testing. In summary, SAF achieves significant performance gains of 12.79% and 4.03% on Minesweeper and Tolokers datasets, respectively, while maintaining competitiveness on the other three.

Table 4: Evaluations on new heterophilic graph datasets.

| Method     | Mine.             | Tolo.             | Amaz.             | Roma.             | Penn94            |
|------------|-------------------|-------------------|-------------------|-------------------|-------------------|
| MLP        | 50.61±0.87        | 74.58±0.69        | 45.50±0.38        | 66.11±0.33        | 74.58±0.37        |
| GCN        | 72.25±0.60        | 76.56±0.85        | 48.06±0.39        | 53.49±0.33        | 82.47±0.27        |
| APPNP      | 68.48±1.20        | 74.13±0.62        | 48.12±0.37        | 72.99±0.46        | 75.29±0.27        |
| GPR-GNN    | 89.76±0.53        | 75.82±0.50        | 49.06±0.25        | 73.19±0.24        | 81.38±0.16        |
| ChebNetII  | 83.62±1.51        | 78.95±0.49        | 49.76±0.36        | 74.52±0.54        | 83.12±0.22        |
| JacobiConv | 89.88±0.33        | 77.24±0.39        | 43.89±0.28        | 74.30±0.50        | 83.35±0.11        |
| NodeFormer | 89.89±0.46        | <b>80.31±0.75</b> | 43.67±1.54        | 73.59±0.60        | 69.66±0.83        |
| GloGNN++   | 72.59±1.54        | 79.01±0.84        | 50.03±0.29        | 66.10±0.26        | 73.15±0.59        |
| FE-GNN     | 84.68±0.36        | 79.31±0.59        | 49.46±0.29        | 74.50±0.30        | 82.30±0.54        |
| BernNet    | 77.75±0.61        | 75.35±0.63        | 49.84±0.52        | 74.56±0.74        | 82.47±0.21        |
| SAF        | <b>90.54±0.30</b> | 79.38±0.58        | <b>50.49±0.28</b> | <b>74.87±0.22</b> | <b>83.86±0.26</b> |
| Improv.    | 12.79%            | 4.03%             | 0.65%             | 0.31%             | 1.39%             |

### F.4 Ablation Study

Table 5 presents detailed ablation study results of SAF framework regarding attention mechanism in “Node-wise Prediction Amalgamation” (Atte.), “Non-negative Spectral Filtering” (Spec.), and “Non-local Spatial Aggregation” (Spat.) modules.

Table 5: Ablation study of SAF framework.

| Our Variant     | Cham. | Squi. | Texas | Corn. | Actor | Cora  | Cite. | Pubm. | Mine. | Tolo. | Amaz. | Roma. |
|-----------------|-------|-------|-------|-------|-------|-------|-------|-------|-------|-------|-------|-------|
| SAF- $\epsilon$ | 74.84 | 64.00 | 94.75 | 93.28 | 42.98 | 89.87 | 81.45 | 91.52 | 90.59 | 79.45 | 50.36 | 74.89 |
| SAF             | 75.30 | 63.63 | 94.10 | 92.95 | 42.93 | 89.80 | 80.61 | 91.49 | 90.54 | 79.38 | 50.49 | 74.87 |
| SAF w/o Atte.   | 75.01 | 62.62 | 89.18 | 86.07 | 41.53 | 88.80 | 80.37 | 91.24 | 89.45 | 76.18 | 49.98 | 74.25 |
| SAF w/o Spec.   | 73.55 | 55.70 | 90.49 | 88.20 | 41.06 | 88.03 | 78.87 | 90.12 | 89.45 | 78.23 | 49.13 | 71.85 |
| SAF w/o Spat.   | 68.53 | 51.39 | 92.62 | 92.13 | 41.71 | 88.51 | 80.08 | 88.51 | 77.75 | 75.35 | 49.84 | 74.56 |

## F.5 Parameter Study

This section presents the sensitivity analysis of hyper-parameters including  $\tau$ ,  $\eta$ ,  $\epsilon$ , and  $L$ . Figure 8 visualizes how varying these parameters within a broad range influences learning performance, showcasing our model’s robust stability over diverse settings. Beyond empirical observation, we also provides deeper insights into parameter understanding and rationalizes the chosen ranges for parameter searching: **1)** The scaling parameter  $\tau = \frac{\alpha}{1-\alpha}$ , crucial in new graph construction in Eq. (6), stems from the trade-off parameter  $\alpha \in (0, 1)$  within the graph optimization problem in Eq. (3). While theoretically we have  $0 = \frac{0}{1-0} < \tau < \frac{1}{1-1} = \infty$ , practical considerations for extracting structural information suggest a larger penalty on the trace objective term  $\text{tr}(\mathbf{Z}^T \gamma_\theta(\hat{\mathbf{L}})\mathbf{Z})$ , i.e., keeping  $\alpha < 0.5$ , thereby limiting  $\tau < \frac{0.5}{1-0.5} = 1$ . This rationale substantiates our selection of  $\tau$  within the set  $\{0.1, 0.2, \dots, 1\}$  as stated in Appendix E.3, aligning with the observed optimal performance in Figures 8(a)-(e). When addressing graphs with noisy structure, we may adjust the upper limit of  $\alpha$  to  $t \in (0, 1)$ , setting  $\tau$ ’s maximum possible value to  $\frac{t}{1-t}$ . For graph benchmarking evaluations in this work, where extracting structural information is important, we practically set  $t = 0.5$ ; **2)** For the non-local aggregation layer number  $L$ , a noticeable decline in model performance is observed when  $L$  exceeds 10. This is attributed to the non-local nature of our new graph, which facilitates efficient information exchange between nodes. Exceeding a certain number of layers may potentially lead to oversmoothing, where there is an overemphasis on global information, thus degrading model performance. However, choosing the number of layers within a reasonable range generally ensures consistent and impressive model performance, as verified in Figures 8(j)-(l).

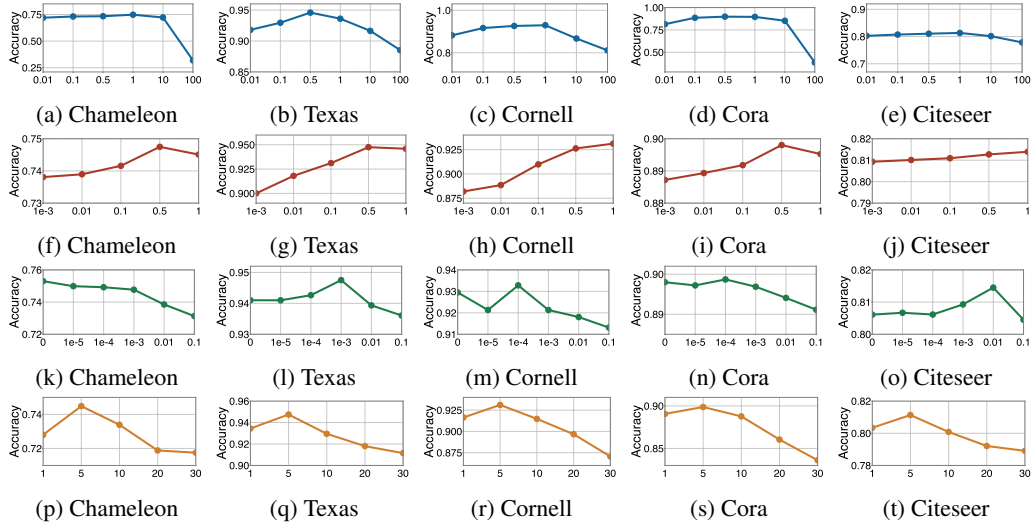


Figure 8: Sensitivity analysis of hyper-parameters:  $\tau$ ,  $\eta$ ,  $\epsilon$ , and  $L$  from top to bottom rows.

Table 6: Full-supervised node classification accuracy (%).

| Method               | Cham.            | Squi.            | Texas            | Corn.            | Actor            | Cora             | Cite.            | Pubm.            |
|----------------------|------------------|------------------|------------------|------------------|------------------|------------------|------------------|------------------|
| ChebNetII            | 71.37 $\pm$ 1.01 | 57.72 $\pm$ 0.59 | 93.28 $\pm$ 1.47 | 92.30 $\pm$ 1.48 | 41.75 $\pm$ 1.07 | 88.71 $\pm$ 0.93 | 80.53 $\pm$ 0.79 | 88.93 $\pm$ 0.29 |
| SAF-Cheb             | 74.97 $\pm$ 0.66 | 64.06 $\pm$ 0.59 | 94.43 $\pm$ 1.81 | 92.62 $\pm$ 2.13 | 42.65 $\pm$ 1.01 | 89.56 $\pm$ 0.64 | 80.68 $\pm$ 0.68 | 91.27 $\pm$ 0.34 |
| SAF-Cheb- $\epsilon$ | 75.25 $\pm$ 0.96 | 64.42 $\pm$ 0.82 | 94.26 $\pm$ 1.64 | 93.12 $\pm$ 1.64 | 42.79 $\pm$ 1.04 | 89.61 $\pm$ 0.71 | 81.08 $\pm$ 0.68 | 91.73 $\pm$ 0.18 |
| Improv.              | 3.88%            | 6.70%            | 1.15%            | 0.82%            | 1.04%            | 0.90%            | 0.15%            | 2.80%            |

## F.6 SAF with ChebNetII as Base Model

To expand the versatility of our SAF framework, we introduced ChebNetII [12] as an alternative base model, chosen for its adherence to the non-negative constraint, critical in our model design as stated in Section 5. The rationale behind this choice is ChebNetII’s use of Chebyshev interpolation for learning Chebyshev polynomials, where the constraint can be ensured by keeping its learnable parameters  $\{\gamma_j\}_{j=0}^K$  non-negative. Our experiments, as shown in Table 6, confirm that SAF can significantly

enhances ChebNetII’s performance, underscoring the framework’s flexibility with different spectral filters. Interestingly, we observed that SAF, utilizing Bernstein polynomials (SAF-Bern), slightly surpasses its performance with Chebyshev polynomials (SAF-Cheb) in most datasets. The margin of improvement over the base model is also more pronounced with SAF-Bern. This phenomenon could be attributed to the  $g_\phi(\lambda) \leq 1$  constraint within SAF (refer to Section 5), necessitating the rescaling of filter functions by their maximum values. For Bernstein polynomials, this maximum is readily obtained as the largest polynomial coefficient  $\max\{\phi_k\}_{k=0}^K$ , as per Proposition 3. However, for Chebyshev polynomials, the best theoretical upper bound is the sum of absolute coefficients,  $\sum_{k=0}^K |\phi_k|$ , which is comparatively less precise. This difference may impact the quality of graph construction and, subsequently, compromise the model’s performance. Exploring these nuances will be a focal point of our future research.

## F.7 Time and Space Overheads

**Eigendecomposition.** Our SAF framework pre-computes eigendecomposition once per graph and reuses it in Eq. (6) in both training and inference. This aspect is crucial, as the forward-pass cost in model training often exceeds the preprocessing expense of eigendecomposition. To empirically validate this, we compare the time overheads of eigendecomposition with the training times of various models in Table 7. Overall, we have following observations: **1)** For datasets with a small number of nodes, the time consumed by decomposition is significantly less than the time required for model training; **2)** For medium-sized graphs such as Pubmed, while the full decomposition time exceeds that of BernNet, it still maintains efficiency against more advanced GNNs such as ChebNetII, NodeFormer and GloGNN++; **3)** Moving to the large-scale graph, Penn94 (with 41,554 nodes and 1,362,229 edges), where only partial eigendecomposition with 100 extremal eigenvalues is considered, the computation time is markedly reduced compared to all the models. For space overheads in Table 8, similar patterns can be observed.

**Model Comparison.** In Table 7, we compare the running times of our SAF against two notable spectral GNNs (BernNet, ChebNetII), two non-local GNNs (NodeFormer, GloGNN++), and one unified GNN model (FE-GNN). Generally, one can observe that SAF, while slightly slower than its base model, BernNet, due to the integration of non-local spatial aggregation, remains more efficient than or comparable to other SOTA methods, particularly those also employing non-local approaches such as NodeFormer and GloGNN++.

Table 7: Time overheads (s).

| Method        | Cham.  | Squi.   | Texas | Corn. | Actor  | Cora  | Cite. | Pubm.   | Penn94    |
|---------------|--------|---------|-------|-------|--------|-------|-------|---------|-----------|
| # Nodes       | 2,277  | 5,201   | 183   | 183   | 7,600  | 2,708 | 3,327 | 19,717  | 41,554    |
| # Edges       | 36,101 | 217,073 | 309   | 295   | 33,544 | 5,429 | 4,732 | 44,338  | 1,362,229 |
| BernNet       | 8.36   | 13.74   | 3.92  | 4.16  | 4.88   | 5.24  | 5.52  | 6.06    | 24.05     |
| ChebNetII     | 22.82  | 30.73   | 11.47 | 9.64  | 14.88  | 19.96 | 16.14 | 36.91   | 41.67     |
| FE-GNN        | 3.99   | 45.89   | 1.03  | 0.84  | 0.98   | 2.54  | 2.06  | 6.78    | 7.33      |
| NodeFormer    | 58.96  | 79.66   | 14.29 | 18.89 | 66.20  | 19.25 | 32.00 | 68.57   | 122.91    |
| GloGNN++      | 35.63  | 68.31   | 4.47  | 3.00  | 73.13  | 32.68 | 12.35 | 5266.53 | 3614.37   |
| SAF           | 11.55  | 18.78   | 4.38  | 4.70  | 5.36   | 6.04  | 6.12  | 18.43   | 23.49     |
| Decomposition | 0.58   | 1.59    | 0.02  | 0.02  | 3.93   | 1.00  | 0.77  | 21.34   | 4.76      |

Table 8: Space overheads (MB).

| Method        | Cham.  | Squi.   | Texas | Corn. | Actor  | Cora  | Cite. | Pubm.  | Penn94    |
|---------------|--------|---------|-------|-------|--------|-------|-------|--------|-----------|
| # Nodes       | 2,277  | 5,201   | 183   | 183   | 7,600  | 2,708 | 3,327 | 19,717 | 41,554    |
| # Edges       | 36,101 | 217,073 | 309   | 295   | 33,544 | 5,429 | 4,732 | 44,338 | 1,362,229 |
| BernNet       | 72     | 232     | 5     | 5     | 292    | 64    | 152   | 1546   | 1902      |
| ChebNetII     | 72     | 231     | 5     | 5     | 291    | 63    | 152   | 1584   | 1850      |
| FE-GNN        | 1337   | 6919    | 23    | 10    | 416    | 302   | 740   | 2213   | 5854      |
| NodeFormer    | 1522   | 3965    | 15    | 37    | 775    | 480   | 764   | 2119   | 3056      |
| GloGNN++      | 290    | 1525    | 5     | 5     | 2471   | 331   | 607   | 17892  | 25260     |
| SAF           | 112    | 440     | 5     | 5     | 733    | 120   | 237   | 4515   | 8491      |
| Decomposition | 141    | 540     | 1     | 1     | 1206   | 140   | 239   | 7641   | 4         |

## **G Societal Impact and Limitations**

This study presents a cross-domain analysis on GNN models, offering a fresh perspective by rethinking spectral GNNs from a spatial lens. The methodology proposed in this paper might have great positive societal impact since it significantly enhances the modeling capabilities of GNNs on complex graph linking patterns. This includes more effective capture of long-range dependencies and better management of heterophilic connections in disassortative graphs, which are commonly observed in real-world applications [36, 42]. While no negative societal impacts have been identified, we acknowledge two limitations of this work: (1) the non-negative constraints of the proposed SAF on graph filters might limit model expressiveness, indicating room for theoretical refinement; (2) although this study focuses on a node-level investigation, it raises intriguing questions about the implications of spectral GNNs at the graph-level in the spatial domain. Future work could expand this examination by relaxing theoretical constraints or exploring the cross-domain interplay from a broader graph-level viewpoint.